Supporting Information for

Mechanical stabilization of a bacterial adhesion

Wenmao Huang[1,2], Shimin Le[1,6], Yuze Sun[2], Dennis Jingxiong Lin[1,2], Mingxi Yao[2,4], Yi Shi[5], Jie Yan[1,2,3]*

[1]*Department of Physics, National University of Singapore, Singapore 117542*

[2]*Mechanobiology Institute, National University of Singapore, Singapore 117411*

[3]*Centre for Bioimaging Sciences, National University of Singapore, Singapore 117546*

[4]*Department of Biomedical Engineering, Southern University of Science and Technology, P.R. China 518055*

[5]*Institute of Materials Research and Engineering, A*STAR, 2 Fusionopolis Way, Innovis, #08-03, Singapore 138634*

[6]*Research Institute for Biomimetics and Soft Matter, Fujian Provincial Key Lab for Soft Functional Materials Research, Department of Physics, Xiamen University, Xiamen 361005, China*

Corresponding Author

*Jie Yan. Email: phyyj@nus.edu.sg

This PDF file includes:

Supporting Methods

Supporting Texts 1−6

Figure S1. Illustration of single-molecule experiment.

Figure S2. Representative traces of SdrG-Fgβ complex at 23 °C.

Figure S3. Force-jumping experiment.

Figures S4–6. Control experiments.

Figure S7. Lifetime histograms of SdrG-Fgβ complex at 23 °C.

Figure S8. Representative traces of SdrG-Fgβ complex at higher forces.

Figures S9–11. Mechanical stability of wild-type SdrG to Fgβ mutants with different number of Phenylalanines.

Figures S12–14. Mechanical stability of wild-type SdrG to Fgβ truncates.

Figures S15 and S16. Mechanical stability of SdrG with mutated "latch" strand to wild-type Fgβ.

Figures S17 and S18. Mechanical stability of SdrG with truncated "latch" strand to wild-type Fgβ.

Figure S19. Representative traces of SdrG-Fgβ complex at 37 °C.

Figures S20–23. Lifetime histograms of SdrG-Fgβ complex at temperature from 26.5 to 37 °C.

Figures S24–30. Mechanical responses of homologues adhesion complexes.

Figure S31. The structural-elastic determinant of the catch-bond kinetics.

Figure S32. Proposed mechanisms of MSCRAMMs-mediated adhesion of the Staphylococcus pathogens.

Tables S1–5

References

Supporting Methods

Channel and microbeads preparation

To measure the mechanical stability of the adhesion protein complex by MT setup, we prepared spy-catcher-functionalized coverslip channels and neutravidin-coated magnetic beads for the formation of a single molecule tether through spy-tag−spy-catcher attachment and biotin−neutravidin cross-linking, respectively.

Cover glasses (32 mm × 22 mm, 0.17 mm thick, Citoglass) were first immersed in detergent (50% Decon 90, Decon Laboratories Limited) overnight then sonicated for 30 minutes. After thoroughly washed with deionized (DI) water, ethanol and acetone successively, these cover glasses were dried under a steam of nitrogen and then treated with oxygen plasma (8%, 50 mW, Tergeo plasma cleaner) for 5 minutes to expose surface hydroxyl groups. These glass substrates were immersed in an anhydrous methanol solution containing 1 % (v/v) APTES at room temperature (R.T.) for 1 hour. Then, they were washed sequentially using methanol and acetone, dried under a nitrogen flow, and incubated at 90 °C for 60 min. Next, the amino-functionalized glass substrate was attached to a clean glass coverslip (18 mm × 18 mm, 0.17 mm thick, Cytoglass) using SecureSeal adhesive sheet (0.12 mm thick, Sigma-Aldrich) to construct a laminar flow channel. This channel was then immersed with Milli-Q water and buffer-exchanged to 1% (v/v) glutaraldehyde solution. After two-hour glutaraldehyde treatment, the channel was gently washed with water followed by 1 × PBS solution. About 100 μL of 1 × PBS solution containing polystyrene beads (1:100 dilution, 2.68 μm amino polystyrene beads, Spherotech) was flowed into the channel. The polystyrene beads were used as references adhered on the surface to eliminate spatial drift during experiments. After incubating for 1 hour, 1 × PBS solution with 25 μg mL^{-1} (2 μM) spy-catcher protein was seeped into the channel. The channel was kept wet and allowed to incubate at room temperature (R.T.) for 4 hours, allowing for the conjugation of spy-catcher protein to the cover glass. Unconjugated proteins were then washed away with 1 × PBS for a few times. Finally, the channel was treated with blocking buffer (1 × PBS, 2% BSA, pH=7.4) at R.T. overnight to prevent non-specific binding in the following experiments. The well-blocked channels were kept wet and stored at 4 °C until use.

Superparamagnetic beads (Dynabeads™ M-270 Epoxy, 2.8 μm, Thermo Scientific) in dimethyl sulfoxide (DMSO) were diluted with 1 × PBS to a final concentration at around 1 mg mL^{-1}. The beads were pulled down by magnets and rinsed with 1 × PBS for three times. 1 × PBS solution containing 50 μg mL^{-1} (0.83 μM) neutravidin protein was added to the epoxy beads suspension. The mixture was kept away from light on a rotator and incubated at R.T. overnight, enabling covalent bond formation of reactive epoxy group to neutravidin protein. After 12 hours, the beads were washed repeatedly with 1 × PBS solution for ~ 5 times and blocked using BSA blocking buffer (1 × PBS, 2% BSA, pH=7.4) on a rotator for 12 hours. The well-blocked neutravidin-coated magnetic beads were stored on a rotator at 4 °C for use.

Sample preparation

All recombinant proteins containing the adhesion complexes were diluted to approximately 1 nM using the standard working buffer (1 × PBS, 1% (m/m) BSA, 1 mM DTT, 10 mM L-ascorbate acid, pH = 7.4) for sample preparation. The spy-catcher-functionalized channel was first washed for a few times with the standard buffer, then the diluted proteins containing spy-tag were introduced into the channel and incubated for 15 minutes, allowing the surface anchorage to occur between the recombinant protein and the channel surface via spy-tag−spy-catcher interaction. The

channel was washed a few times to remove unbounded proteins. Next, an adequate amount of neutravidin-coated superparamagnetic beads was added into the channel and allowed to incubate for 15 minutes. Finally, the channel was sealed completely using mineral oil to mitigate the effects of solution evaporation during the long-time experiment. The channel was then transferred and mounted onto the magnetic-tweezer setup to proceed with the experiment.

Magnetic tweezer setup and force-jumping experiment

The home-made magnetic tweezer was built on an inverted microscope (IX71, Olympus). 100 × oil-immersion objective (UPlanFLN 100X, Olympus) was used to monitor images of the protein-tethered bead. An image library at a series of different focal planes was built through adjusting the focal plane of objective by a piezo objective actuator (E-753 Digital Piezo Controller, PI). Two permanent magnetic rods were placed vertically above the channel, whose movement was controlled by a motorized stage (VT-40, Micos) to change the magnetic force applied to the sample. By adopting a high FOV camera (Basler acA1920-155 μm), multiple magnetic beads could be tracked and monitored in real-time. During the measurements, the height changes of the magnetic beads compared to the fixed reference beads, which corresponded to the extension of the protein tether, were recorded. The piezo objective actuator was used to correct the drift of focal plane in real time by monitoring drift of the reference bead, which provided a long-term ultrastability of the magnetic tweezer setup.

In a typical force jumping experiment, the magnet was jumped from approximately 1.5 pN to a constant testing force in the range of 3−50 pN. The bead height-time traces of the tethers were recorded in real-time. A feedback function monitoring the bead height change was added into the Labview controlling program to automatically reduce the magnetic force down to ~1.5 pN once the protein complex was dissociated, where the bead height jumped to a greater value. The force was then increased to the testing constant force for the next cycle once the protein adhesion complex was reformed. Collectively, by using this ultra-stable magnetic tweezer setup, we were able to record data from multiple tethers under constant force over a period of few days. As for the temperature dependent experiment, the objective heating system was turned on to increase the channel temperature for 1 hour to establish a thermal equilibrium prior to measurement.

Force calibration

Force calibration was conducted for each tethered bead measured in the experiments, which had ~10 % relative error[1,2]. The force applied to a bead is a function of the distance (d) between permanent magnets and the paramagnetic beads, which was calibrated by 16 μm λ-DNA as described in our previous publication[1]. For the magnets pair we used in the manuscript, the force equation is given by[1]:

$$f = C * \left(exp\left(-\frac{d}{0.36}\right) + 0.48exp\left(-\frac{d}{1.12}\right)\right) \qquad \text{Eq. 1}$$

where d is in unit of millimeter, and C value is a constant which differs for each paramagnetic bead. For the M270 beads, the C value is in the range of 180−210 pN.

For each individual tethered bead measured in experiments, the force was calibrated by the bead fluctuation at forces < 10 pN by[1,2]:

$$f = \frac{k_B T(R+z)}{\delta_y{}^2} \qquad \text{Eq. 2}$$

where $k_B T$ is the Boltzmann constant times temperature, R is the radius of the paramagnetic bead (1.4 μm for typical M270 Dynabead), z is the extension of tether, and $\delta_y{}^2$ is the variance of transverse fluctuation of the magnetic bead perpendicular to the magnetization direction. The

calibrated forces were extrapolated to higher forces through Eq. 1. Due to the uncertainty of bead size and the deviation of tether point from the bottom pole of the bead, the calibrated forces have about 10% relative error.

Force-extension curves

Due to the potential rotation of the tethered magnetic beads under force, the absolute bead height is not the extension of the short-tethered proteins[2]; while the extension change (steps size, $\Delta x(f)$) at a constant force (f) can be accurately measured. The force-extension curves ($x(f)$) of the ruptured adhesion complex and the unfolded peptides of N2, N3 domain can be obtained from $\Delta x(f)$ by:

$$x(f) = \Delta x(f) + x_0(f) \qquad \text{Eq. 3}$$

where $x_0(f)$ is the force-extension of the adhesion complex or the folded N2, N3 domain. At a low-force region, $x_0(f)$ is simplified to a constant and measured from the PDB structures.

The force-extension curves of the ruptured adhesion complex and the unfolded peptides of N2, N3 domain can be modeled as a worm-like chain (WLC) polymer and described by the Marko-Siggia formula[3]:

$$\frac{fA}{k_bT} = \frac{1}{4(1-x(f)/L)^2} + \frac{x(f)}{L} - \frac{1}{4} \qquad \text{Eq. 4}$$

where A is the persistence length and L is the contour length of polymer. At a low-force region, the force-extension (x_0) of SdrG-Fgβ complex and the folded N2, N3 domain along the force direction are 5.0 nm, ~ 5.0 nm, ~ 8.0 nm by measuring the crystallized structure (PDB 1r17), respectively. The A and L value of the ruptured SdrG-Fgβ complex and the unfolded peptides of N2, N3 domain were obtained by fitting the extension changes at different forces with Eq. 4 (Figure S5). The contour length L was further converted to the number of amino acid (L ~ 0.36 nm per amino acid,[4]).

Protein construction and sequence

The full amino acid sequence of the protein construction used in this work are listed below. All sequences contain a 6×HIS (HHHHHH) tag for purification, an avi-tag (GLNDIFEAQKIEWHE) for biotinylation, and a spy-tag (AHIVMVDAYKPTK) for surface covalent functionalization.

SdrG(N2N3)-Fgβ wild-type: Fgβ-avi-GSlinker-SdrG(N2N3)-spy

MNEEGFFSARGHRPLDHHHHHHGKPIPNPLLGLDSTENLYFQGIDPFTGLNDIFEAQ
KIEWHESGEFGSGSSGSGSGGSSGSGGSSGSGSSGSGSSGSSGSSGSGSGGSGSSGSGGGG
SSGSGSSGSSGSGSGGGSGSGSSGLESGSGSSGSGSGGSSGSGGSSGSGSSGSGSSGSSGSS
GSGSGGSGSSGSGGGGSSGSGSSGSSGSGSGGGSGSGSSGGSEQGSNVNHLIKVTDQSIT
EGYDDSDGIIKAHDAENLIYDVTFEVDDKVKSGDTMTVNIDKNTVPSDLTDSFAIPKIKD
NSGEIIATGTYDNTNKQITYTFTDYVDKYENIKAHLKLTSYIDKSKVPNNNTKLDVEYKT
ALSSVNKTITVEYQKPNENRTANLQSMFTNIDTKNHTVEQTIYINPLRYSAKETNVNISG
NGDEGSTIIDDSTIIKVYKVGDNQNLPDSNRIYDYSEYEDVTNDDYAQLGNNNDVNINF
GNIDSPYIIKVISKYDPNKDDYTTIQQTVTMQTTINEYTGEFRTASYDNTIAFSTSSGQGQ
GDLPPEGGGSGAHIVMVDAYKPTK

SdrG(N2N3): avi-GSlinker-SdrG(N2N3)-spy

MHHHHHHGKPIPNPLLGLDSTENLYFQGIDPFTGLNDIFEAQKIEWHESGEFGSGSS
GSGSGGSSGSGGSSGSGSSGSGSSGSGSSGSGSGGSGSSGSGGGGSSGSGSSGSSGSGSG
GGSGSGSSGLESGSGSSGSGSGGSSGSGGSSGSGSSGSGSSGSSGSGSGGSGSSGSGG
GGSSGSGSSGSSGSGSGGGGSGSGSSGGSEQGSNVNHLIKVTDQSITEGYDDSDGIIKAHD
AENLIYDVTFEVDDKVKSGDTMTVNIDKNTVPSDLTDSFAIPKIKDNSGEIIATGTYDNT
NKQITYTFTDYVDKYENIKAHLKLTSYIDKSKVPNNNTKLDVEYKTALSSVNKTITVEY
QKPNENRTANLQSMFTNIDTKNHTVEQTIYINPLRYSAKETNVNISGNGDEGSTIIDDSTII
KVYKVGDNQNLPDSNRIYDYSEYEDVTNDDYAQLGNNNDVNINFGNIDSPYIIKVISKY
DPNKDDYTTIQQTVTMQTTINEYTGEFRTASYDNTIAFSTSSGQGQGDLPPEGGGSGAHI
VMVDAYKPTK

SdrG(N2N3)-FH1-Fgβ: Fgβ-avi-FH1linker-SdrG(N2N3)-spy

MNEEGFFSARGHRPLDHHHHHHGKPIPNPLLGLDSTENLYFQGIDPFTGLNDIFEAQ
KIEWHESGEFPPAPPLPGDSGTIIPPPPAPGDSTTPPPPPPPPPPPPLPGGVCISSPPSLPGGT
AISPPPPLSGDATIPPPPPLPEGVGIPSPSSLPGGTAIPPPPPLPGSARIPPPPPPLPGSAGIPPPP
PPLPGEAGMPPPPPPLPGGPGIPPPPPFPGGPGIPPPPPGMGMPPPPPFGFGVPAAPVLPGSE
QGSNVNHLIKVTDQSITEGYDDSDGIIKAHDAENLIYDVTFEVDDKVKSGDTMTVNIDK
NTVPSDLTDSFAIPKIKDNSGEIIATGTYDNTNKQITYTFTDYVDKYENIKAHLKLTSYID
KSKVPNNNTKLDVEYKTALSSVNKTITVEYQKPNENRTANLQSMFTNIDTKNHTVEQTI
YINPLRYSAKETNVNISGNGDEGSTIIDDSTIIKVYKVGDNQNLPDSNRIYDYSEYEDVTN
DDYAQLGNNNDVNINFGNIDSPYIIKVISKYDPNKDDYTTIQQTVTMQTTINEYTGEFRT
ASYDNTIAFSTSSGQGQGDLPPEGGGSGAHIVMVDAYKPTK

Fgβ ligand mutations (mutations along the Fgβ are listed below compared to the Fgβ wild-type, the other regions are all the same as SdrG(N2N3)-Fgβ wild-type**):**

Fgβ wild-type (or FgβF2): NEEGFFSARGHRPLD
FgβF1: NEEGAFSARGHRPLD
FgβF0: NEEGAASARGHRPLD
FgβF3: NEEGFFFSARGHRPLD
FgβFFSARG: FFSARGGSGSG
FgβdN4: FFSARGHRPLD
FgβdC5: NEEGFFSARGGSGSG

*For **FgβFFSARG** and **FgβdC5**, in order to maintain the force geometry applied to the ligand after truncation, five amino acids (GSGSG) were used to replace the HRPLD in the C terminal of Fgβ ligand.

SdrG(N2N3) mutations (mutations along the C-terminus of the "latch" strand of N3 domain are listed below compared to the wild-type latching strand, the other regions are all identical to SdrG(N2N3)-Fgβ wild-type**):**

SdrG(N2N3) wild-type: STSSGQGQGDLPPE
SdrG(N2N3)_D593A: STSSGQGQGALPPE
SdrG(N2N3)_G592A&D593A: STSSGQGQAALPPE

SdrG(N2N3)_dC11: STS
SdrG(N2N3)_dC8: STSSGQ

SdrE(N2N3)-CFH: CFH-avi-GSlinker-SdrE(N2N3)-spy

MRLSSRSHTLRTTCWDGKLEYPHHHHHHGKPIPNPLLGLDSTENLYFQGIDPFTGL
NDIFEAQKIEWHESGEFGSGSSGSGSGGSSGSGGSSGSGSSGSGSSGSSGSSGSGSGGSGS
SGSGGGGSSGSGSSGSSGSGSGGGSGSGSSGLESGSGSSGSGSGGSSGSGGSSGSGSSGSG
SSGSSGSSGSGSGGSGSSGSGGGGSSGSGSSGSSGSGSGGGSGSGSSGGSAVAQPAAVAS
NNVNDLIKVTKQTIKVGDGKDNVAAAHDGKDIEYDTEFTIDNKVKKGDTMTINYDKNV
IPSDLTDKNDPIDITDPSGEVIAKGTFDKATKQITYTFTDYVDKYEDIKSRLTLYSYIDKKT
VPNETSLNLTFATAGKETSQNVTVDYQDPMVHGDSNIQSIFTKLDEDKQTIEQQIYVNPL
KKSATNTKVDIAGSQVDDYGNIKLGNGSTIIDQNTEIKVYKVNSDQQLPQSNRIYDFSQY
EDVTSQFDNKKSFSNNVATLDFGDINSAYIIKVVSKYTPTSDGELDIAQGTSMRTTDKYG
YYNYAGYSNFIVTSNDTGGGDGTVKPEEKGGGSGAHIVMVDAYKPTK

Bbp(N2N3)-Fgα: Fgα-avi-GSlinker-Bbp(N2N3)-spy

MSKQFTSSTSYNRGDSHHHHHHGKPIPNPLLGLDSTENLYFQGIDPFTGLNDIFEAQ
KIEWHESGEFGSGSSGSGSGGSSGSGGSSGSGSSGSGSSGSSGSGSGGSGSSGSGGGG
SSGSGSSGSSGSGSGGGSGSGSSGLESGSGSSGSGSGGSSGSGGSSGSGSSGSGSSGSS
GSGSGGSGSSGSGGGGSSGSGSSGSSGSGSGGGSGSGSSGGSASNNVNDLITVTKQMITE
GIKDDGVIQAHDGEHIIYTSDFKIDNAVKAGDTMTVKYDKHTIPSDITDDFTPVDITDPSG
EVIAKGTFDLNTKTITYKFTDYVDRYENVNAKLELNSYIDKKEVPNETNLNLTFATADK
ETSKNVKVEYQKPIVKDESNIQSIFSHLDTTKHEVEQTIYVNPLKLNAKNTNVTIKSGGV
ADNGDYYTGDGSTIIDSNTEIKVYKVASGQQLPQSNKIYDYSQYEDVTNSVTINKNYGT
NMANINFGDIDSAYIVKVVSKYTPGAEDDLAVQQGVRMTTTNKYNYSSYAGYTNTILS
TTDSGGGDGTVKPEEKGGGSGAHIVMVDAYKPTK

ClfB(N2N3)-DK: ClfB(N2N3)-spy-GSlinker-avi-DK

MHHHHHHGTNVNDKVTASNFKLEKTTFDPNQSGNTFMAANFTVTDKVKSGDYFT
AKLPDSLTGNGDVDYSNSNNTMPIADIKSTNGDVVAKATYDILTKTYTFVFTDYVNNKE
NINGQFSLPLFTDRAKAPKSGTYDANINIADEMFNNKITYNYSSPIAGIDKPNGANISSQII
GVDTASGQNTYKQTVFVNPKQRVLGNTWVYIKGYQDKIEESSGKVSATDTKLRIFEVN
DTSKLSDSYYADPNDSNLKEVTDQFKNRIYYEHPNVASIKFGDITKTYVVLVEGHYDNT
GKNLKTQVIQENVDPVTNRDYSIFGWNNENVVRYGGGSADGDSAVGKLSGAHIVMVD
AYKPTKSGEFGSGSSGSGSGGSSGSGGSSGSGSSGSGSSGSSGSSGSGSGGSGSSGSGGG
GSSGSGSSGSSGSGSGGGSGSGSSGLESGSGSSGSGSGGSSGSGGSSGSGSSGSGSSGSSG
SSGSGSGGSGSSGSGGGGSSGSGSSGSSGSGSGGGSGSGSSGGSGLNDIFEAQKIEWHEG
KPIPNPLLGLDSTQSGSSGSGSNGD

ClfA(N2N3)-Fgγ: ClfA(N2N3)-spy-GSlinker-avi-Fgγ

MHHHHHHGAPVAGTDITNQLTNVTVGIDSGTTVYPHQAGYVKLNYGFSVPNSAV
KGDTFKITVPKELNLNGVTSTAKVPPIMAGDQVLANGVIDSDGNVIYTFTDYVNTKDDV

KATLTMPAYIDPENVKKTGNVTLATGIGSTTANKTVLVDYEKYGKFYNLSIKGTIDQID
KTNNTYRQTIYVNPSGDNVIAPVLTGNLKPNTDSNALIDQQNTSIKVYKVDNAADLSES
YFVNPENFEDVTNSVNITFPNPNQYKVEFNTPDDQITTPYIVVVNGHIDPNSKGDLALRS
TLYGYNSNIIWRSMSWDNEVAFNNGSGSGDGIDKPVVPEQPGKLSGAHIVMVDAYKPT
KSGEFGSGSSGSGSGGSSGSGGSSGSGSSGSGSSGSSGSSGSGSGGSGSSGSGGGGSSGSG
SSGSSGSGSGGGSGSGSSGLESGSGSSGSGSGGSSGSGGSSGSGSSGSGSSGSSGSSGSGS
GGSGSSGSGGGGSSGSGSSGSSGSGSGGGSGSGSSGGSGLNDIFEAQKIEWHESGSGSGT
GSGSGGEGQQHHLGGAKQAGDV

FnbpA(N2N3)-Fgγ: FnbpA(N2N3)-spy-GSlinker-avi-Fgγ

MHHHHHHGSNAKVETGTDVTSKVTVEIGSIEGHNNTNKVEPHAGQRAVLKYKLKF
ENGLHQGDYFDFTLSNNVNTHGVSTARKVPEIKNGSVVMATGEVLEGGKIRYTFTNDIE
DKVDVTAELEINLFIDPKTVQTNGNQTITSTLNEEQTSKELDVKYKDGIGNYYANLNGSI
ETFNKANNRFSHVAFIKPNNGKTTSVTVTGTLMKGSNQNGNQPKVRIFEYLGNNEDIAK
SVYANTTDTSKFKEVTSNMSGNLNLQNNGSYSLNIENLDKTYVVHYDGEYLNGTDEVD
FRTQMVGHPEQLYKYYYDRGYTLTWDNGLVLYSNKANGNEKNGPIGKLSGAHIVMVD
AYKPTKSGEFGSGSSGSGSGGSSGSGGSSGSGSSGSGSSGSGSSGSGSSGSGGSGSSGSGGG
GSSGSGSSGSSGSGSGGGSGSGSSGLESGSGSSGSGSGGSSGSGGSSGSGSSGSGSSGSSG
SSGSGSGGSGSSGSGGGGSSGSGSSGSSGSGSGGGSGSGSSGGSGLNDIFEAQKIEWHES
GSGSGTGSGSGGEGQQHHLGGAKQAGDV

Supporting Texts

1. Three stepwise jumps in the time trace correspond to dissociation of the complex, followed by the unfolding of the N3, N2 domains

Three jumps of the bead height changes were observed in the time trace of SdrG-Fgβ construct under different applied forces (Figure 1C, Figure S2). In order to distinguish the correspondence of these jumps, we measured the force-dependent step sizes (ΔH_{1-3}) of the time traces from multiple tethers. The force-dependent step sizes were fitted using worm-like chain model (Figure S5), from which the number of the amino acids involved in the released peptides were estimated to be 143, 149, and 118 (amino acids, a.a.), which are consistent with those from the dissociation of the complex and the unfolding of N3 and N2 domains, respectively. When the Fgβ ligand was removed from the protein construct, the dissociation step disappeared, leaving the two unfolding steps remained (Figure S4). To exclude the possible interference of the GS-rich peptide linker, we replaced the GS linker with another well characterized unstructured peptide, the FH1 (182 a.a.) region from formin[5] as a control. Similar three-step bead height jumps were observed (Figure S6). The FH1 region has more amino acid number and is stiffer than the GS linker, resulting in a larger step size of ΔH_1. All results confirmed that the observable three stepwise jumps corresponded to the dissociation of the complex, followed by the unfolding of the N2, N3 domains.

2. Ultra-long lifetime of the complex at higher forces

At 20.0 ± 2.0 pN at 23 °C, the lifetime of SdrG-Fgβ complex exceeds ~ 20 000 s. We carried out further experiments at higher forces of 30.0 ± 3.0 pN or 50.0 ± 5.0 pN. A representative time trace at 30.0 ± 3.0 pN is shown in Figure S8a, where three jumps of the bead height changes were observed after more than 100 000 s. Such an ultra-slow dissociation prevented us from obtaining enough number of rupturing events for statistics analysis. We were only able to collect four rupturing events at this force, resulting in a rough average lifetime of 124 486.4 ± 70 963.5 s (mean ± S.D.). A representative time trace at 50.0 ± 5.0 pN in Figure S8b showed no rupturing event prior to the tether breaking after more than 400 000 s. For all the tethers we tested (> five tethers), no dissociation was observed until tether broken after 150 000 – 500 000 s . Based on these observations, we could conclude that the lifetime of the complex further increased drastically at forces greater than 20 pN and did not show any drops at the highest tested force of ~50 pN. Additionally, we also performed experiments at higher force at 100.0 ± 10.0 pN or 140.0 ± 14.0 pN (Figure S8c-d). No dissociation events were observed for all tested tethers before the breakage of the tethers. At these high forces over 100 pN, the other part of the tether (especially the non-covalent biotin-avidin interaction) are easier to rupture, which led us be unable to maintain the tether for longer time.

3. Adhesion complex formation at ~ 1.5 pN

In a typical force-jumping experiment, the applied force was switched between a testing force (*i.e.* 3−30 pN) and a resting force of 1.5 ± 0.2 pN. Holding the tether at the resting force for a certain waiting time, the complex formation probability was obtained by the fraction of the cycles where the complex was formed. At the resting force, the wild-type SdrG-Fgβ complex can reform in seconds (Figure S3). The refolding of the N2 and N3 domains is much faster than the binding of Fgβ ligand; therefore, the rate limiting step is the ligand binding step. We found that the complex formation probability of the FgβF0 binding to SdrG drops to near zero. The time trace only showed two bead height jumps corresponding to the unfolding of N2 and N3 domain (Figure S9). This

could be explained by an unstable complex of FgβF0-SdrG where the lifetime is too short to be captured at our sampling rate (200 Hz). Mutations (D593A, G592A+D593A) and truncations (SdrG_dC8, SdrG_dC11) on the "latch" strand also gradually reduced the probability of the complex formation after 10 s duration at ~ 1.5 pN (Figure S17). For SdrG_dC11 construct, the time trace only showed two bead height jumps corresponding to the unfolding of N2 and N3 domain, while no complex formation was observed. For SdrG_dC8 construct, the complex formation probability drops ~50% compared to wild-type (Figure S17). Consistently, longer stepwise drops when the force jumped back to 1.5 pN were also observed in the time trace (Figure S17B), indicative of an slower complex formation for SdrG_dC8 construct.

4. The transition pathway at the low-force range

The perturbations on the "latch" strand led to reduced extrapolated zero-force lifetime (τ_0) and decreased magnitude of the transition distance ($\Delta x^{\ddagger}$) compared to the wild-type complex. A shorter τ_0 suggests reduced activation energy (energy barrier height) required for the transition at zero force, due to an overall weaker interaction between the "latch" strand of the mutants to N2 domain. The gradually decreased magnitude of $\Delta x^{\ddagger}$ with the decreased residue number of "latch" strand ($\Delta x^{\ddagger} = -1.20 \pm 0.07$ nm (wild-type), $\Delta x^{\ddagger} = -1.08 \pm 0.05$ nm (D593A), $\Delta x^{\ddagger} = -0.87 \pm 0.10$ nm (G592A+D593A), $\Delta x^{\ddagger} = -0.68 \pm 0.04$ nm (SdrG_dC8)) suggests that the extension difference between the transition state structure and the natively bound state becomes shorter and shorter at low-force range. While the complex is tightened by applied shear force, there are no chances that the unbinding of the "latch" strand could start from the residue in the middle of the strand. Thus, the unbinding of the "latch" strand likely starts from the C-terminal region of the "latch" strand (D593). Overall, these results point out a picture that during the transition, the bonded residues in the "latch" strand are progressively unbinding from the N2 domain until reaching the transition state. Such mechanism has also been found in several force-dependent unfolding transition pathways of protein[6-8] and strand-separation transitions of dsDNA[9,10].

It should be noted that the truncations (SdrG_dC8, SdrG_dC11) on the "latch" region of our protein constructs were done by direct removal of the residues. Consequently, the short peptide linker and spy-tag in the C-terminus of the protein construct would have occupied the previous positions of the truncated "latch" residues. This presents a scenario where the following short linker or spy-tag may form new interactions with the N2 binding cleft interface. This possibility could explain the abnormal phenomenon of SdrG_dC8, where the force-dependent lifetimes are longer than G592A+D593A (Figure 2H in the Main text).

5. Temperature-dependent transition pathway

The drastically decreased τ_0 of the wild-type SdrG-Fgβ complex at increased temperature implies a decreased energy barrier at higher temperature. The drastically decreased lifetimes at increased temperature is unexpected assuming that the nature of transition is identical from 23 to 37 °C. By applying the Arrhenius law, $k(f) \propto \mathrm{e}^{-\frac{\Delta H^{\ddagger}}{k_B T}}$, where $\Delta H^{\ddagger}$ is the activation energy (*i.e.* enthalpy difference of the transition state and the native state), a temperature change from 23 to 37 °C should result in a negligible change of the $\frac{\Delta H^{\ddagger}}{k_B T}$ by around $0.0002\frac{\Delta H^{\ddagger}}{k_B T}$, which cannot explain the drastically changes of the lifetimes by more than 100 folds. On the other hand, the gradual decreased magnitude of the transition distance suggests that the distance along the force direction of the transition state and the native state becomes shorter with increased temperature. We have identified the transition pathway as the sequential unbinding of the "latch" strand from the N2

domain until reaching the transition state. On the basis of this transition pathway and taking into account the dynamics of bond breaking and annealing at the fork between the "latch" peptide and N2 domain[11], we propose that at higher temperature, the association of the C-terminal region of the "latch" strand to the N2 domain becomes more dynamic than that at lower temperatures, resulting in a change of $\Delta H^{\ddagger}$ as well as $\Delta x^{\ddagger}$ that could cause the observed sensitive temperature dependence of lifetime. We note that this explanation does not exclude other possibilities such as the change of transition pathway at different temperatures.

6. Physical mechanism of the catch-bond kinetics

In general, catch-bond dissociation kinetics can be discussed based on Arrhenius law, $\tau(f) = \tau_0 e^{\Delta G^*(f)/k_B T}$, where τ_0 is the zero-force lifetime, T is the temperature, k_B is the Boltzmann constant, and $\Delta G^*(f)$ is the force-dependent free energy barrier, namely the free energy difference between the transition state and native state[12]. Decomposing $\Delta G^*(f)$ into the enthalpy and entropy differences, $\Delta G^*(f) = \Delta H^*(f) - T\Delta S^*(f)$, the catch-bond kinetics can be explained by increased enthalpy difference $\Delta H^*(f)$, or decreased entropy difference $\Delta S^*(f)$, or both, when force increases. Recent studies have revealed that entropic extension fluctuation of biomolecules at forces of pN to tens of pN has a significant impact on $\tau(f)$[13-15], without assuming significant changes in $\Delta H^*(f)$. Based on force-dependent extension difference between the transition state and the native state, a recent theory predicts a force-dependent lifetime of biomolecular complexes, $\tau_0 e^{-(\sigma f - \eta\sqrt{f})/\mathrm{k_B}T}$, which links $\tau(f)$ to the elastic-structural properties of the biomolecular complex. Here, the two parameters, σ and η, are related to the structural-elastic properties via the following equations, $\sigma = (b^* - b_0) + L^*$ and $\eta = L^* \sqrt{\frac{k_B T}{A}}$, where $b^* - b_0$ is the rigid body length difference in the folded cores between the transition and the native state structures, L^* is the contour length of protein peptide produced at the transition state under force, and A is the bending persistence length of the peptide which typical lies in range from 0.5 – 0.8 nm depending on the sequences and solution conditions[15]. The equation predicts catch-bond kinetics if the transition is along a pathway involving unbinding of a pre-extended flexible peptide in the native state from the remaining folded core under a shear-force stretching geometry[16], which results in a negative $\sigma f - \eta\sqrt{f}$, hence catch-bond kinetics, at sufficiently low forces. The more the peptide is pre-extended in the native state, the stronger the catch-bond kinetics. This is exactly the case of the force-dependent SdrG-Fgβ dissociation at the low-force range, where detaching of the highly pre-extended "latch" strand ((> 90% of the contour length) from the N2 domain is involved in the transition suggested by our experimental results.

Indeed, the force-dependent lifetime of the SdrG-Fgβ complex can be well fitted by the elastic-structural model (Figure S31). In this fitting, the structure of the natively bound complex is obtained from the crystal structure of the complex formed between SdrG(N2,N3) and Fgβ ligand (PDB 1r17), from which the value of b_0 was obtained (Figure S31). Assuming the transition state structure corresponds to unbinding of n^* residues from the C-terminal of the "latch" strand, the corresponding b^*, L^* for a set of testing value of $n^* = 1, 2, 3, \ldots, 10$ are measured and listed in Table S2. By fitting to the force-dependent lifetime of SdrG-Fgβ complex, we found that the best-fitted A value at $n^* = 7, 8, 9$ located in the reasonable range of the peptide persistence length (Table S2). Additionally, we have further fitted the force-dependent lifetime of D593A and D593A+G592A mutants using the elastic-structural model. By assuming the mutations totally disrupting the interaction of the D593 and G592 of "latch" strand to N2 domain, the transition state structure corresponds to dissociation of $n^* - 1$ and $n^* - 2$ residues from the C-terminal of the

"latch" strand for D593A and D593A+G592A mutant, respectively. We found that the best-fitted A value at $n^* - 1 = 7, 8$ for D593A and $n^* - 2 = 5, 6$ for D593A+G592A located in the reasonable range of the peptide persistence length (Figure S31d-e, Table S3, S4). These are all consistent with a transition state structure where most of the "latch" strand (7-9 amino acids from the last binding residue, 593D) is dissociated away from the N2 domain (Figure S31). Therefore, while other mechanisms cannot be excluded, the observed strong catch-bond dissociation kinetics over the low-force range can be explained by this mechanism.

Supporting Figures

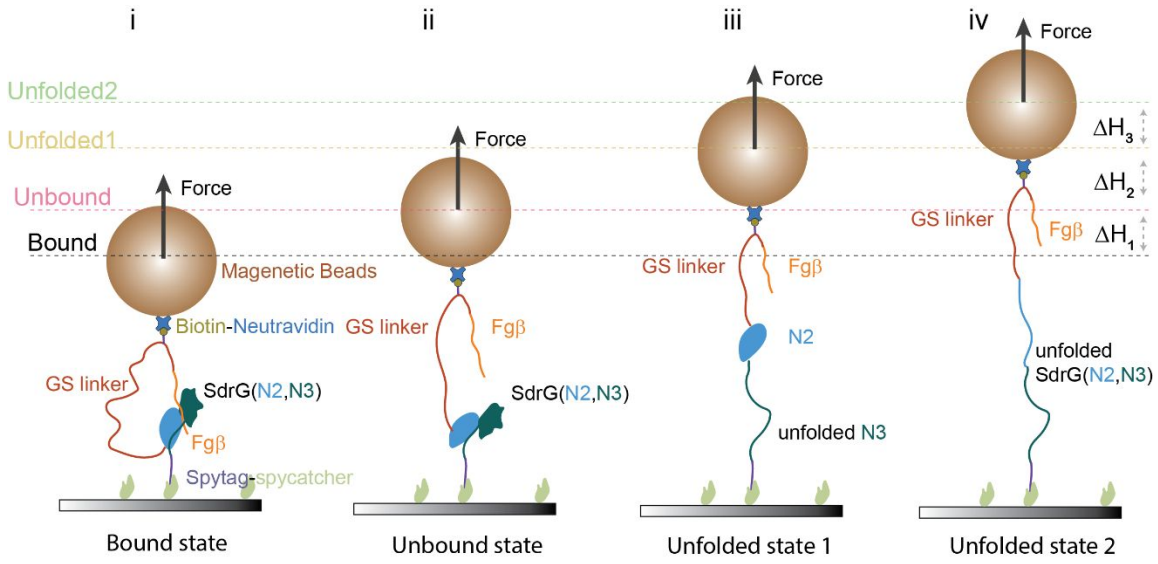

Figure S1. The schematic illustration of a tethered recombinant protein construct containing the SdrG-Fgβ complex under force. An external force is applied by controlling the distance from magnets to the M270 microbead. (i) In the native bound state of SdrG-Fgβ complex, force is applied to the C termini of both Fgβ and N3 domain, where the flexible GS linker is not under force. (ii) Once the Fgβ is ruptured from the N2-N3 binding pocket of SdrG, the released GS linker would give a rise to the extension of the protein construct, leading to an increased height of the bead (ΔH_1). At this unbound state, the N2 and N3 domain is under force pulled from the N-terminus of N2 domain and C-terminus of N3 domain. (iii-iv) Subsequently, the unfolding of N3 and N2 domain contributes to the further stepwise increase of the bead height (ΔH_2,ΔH_3), respectively.

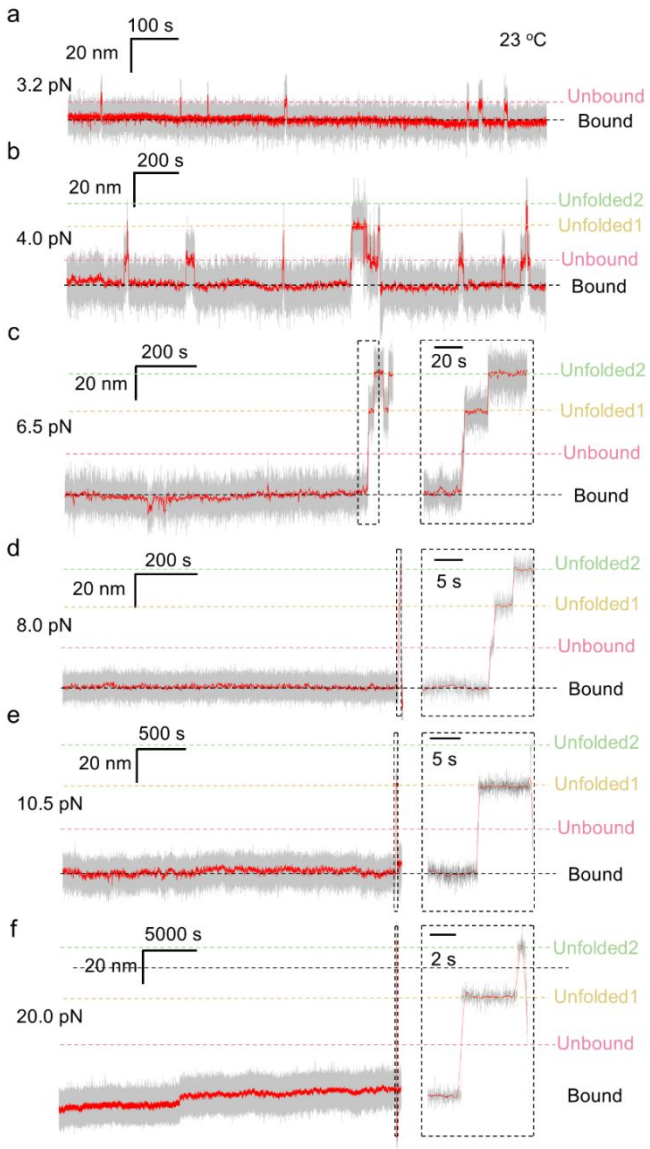

Figure S2. Representative bead height-time traces of the protein construct containing SdrG-Fgβ complex under force range from 3.2 pN to 20.0 pN. (a) Representative bead height-time trace at 3.2 ± 0.4 pN. Single step jump between the bound state and unbound state was obtained, while the two jumps corresponding to the unfolding of the N2, N3 domain were rarely observed at this force. Representative bead height-time traces at (b) 4.0 ± 0.4 pN, (c) 6.5 ± 0.7 pN, (d) 8.0 ± 0.8 pN, (e) 10.5 ± 1.1 pN, and (f) 20.0 ± 2.0 pN are shown with three stepwise jumps corresponding to the transitions of the dissociation of SdrG-Fgβ complex (from bound to unbound state), and two unfolding of the N2, N3 domain of SdrG. Right panels of (c)−(f) are the enlarged time traces around the step jumping transitions. Raw data and smoothed data using Fast Fourier Transform (FFT) with 50 points of window are indicated by gray and red, respectively.

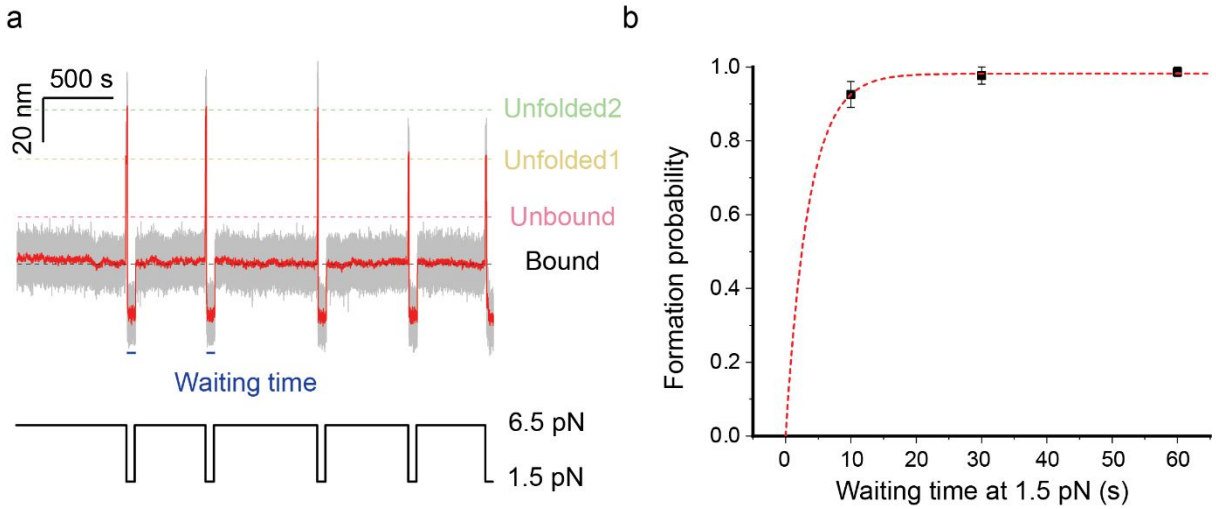

Figure S3. Force-jumping cycles allowing the recording of multiple dissociation and formation events of SdrG-Fgβ complex. (a) A representative time trace containing multiple dissociation and formation events of SdrG-Fgβ complex in force-jumping cycles at 23 ºC. Raw data and smoothed data using FFT with 50 points of window are indicated by gray and red, respectively. The external force is jumping automatically cycling between a testing force of 6.5 ± 0.7 pN, which is to measure the mechanical stability of the complex at this force, and a resting force of 1.5 ± 0.2 pN, which is to allow the formation of the complex once the dissociation stepwise bead height change is detected. By repeating such force-jumping operations on multiple molecules for multiple cycles, the lifetime of the complex at each force and the probability of the complex formation (indicated by the bead height of the next round) after a waiting time at the resting force can be obtained. (b) Complex formation probabilities of SdrG-Fgβ were measured after waiting times of 10 s, 30 s, and 60 s at 1.5 pN, respectively, showing fast formation of the complex in seconds at 1.5 ± 0.2 pN. Error bars indicate mean ± S. D.

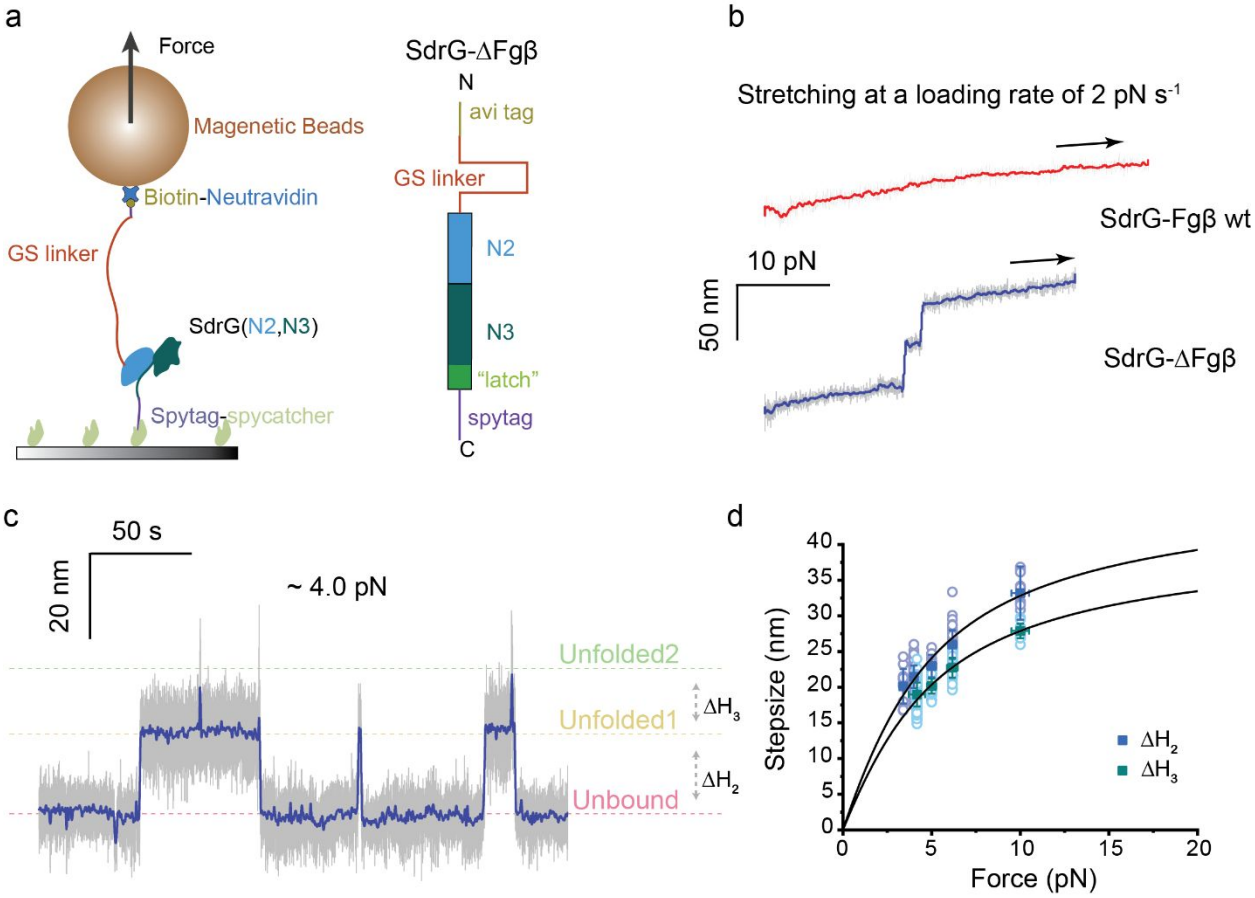

Figure S4. Mechanical signature of the Fgβ truncated protein construct (SdrG-ΔFgβ). (a) Left panel: the schematic diagram of single-molecule magnetic tweezer experiment. Right panel: the schematic illustration of the design of SdrG-ΔFgβ construct where the ligand was removed from the protein construct. (b) Representative force-extension curves of the wild-type SdrG-Fgβ (top) compared to SdrG-ΔFgβ (bottom) at a constant loading rate of 2.0 pN s^{-1}. (c) Representative bead height-time trace of SdrG-ΔFgβ complex at 4.0 ± 0.4 pN. Two stepwise jumps are shown and corresponded to the unfolding of the N2, N3 domain of SdrG, respectively. The step sizes (ΔH_2 , ΔH_3) were obtained by the difference of the peaks in the histogram of bead height distribution of the time trace (not shown). (d) Step sizes of the two bead height jumps (blue: ΔH_2, green: ΔH_3) observed in the time traces at different constant force collected from four different tethers. Raw data are presented as light blue or light green circles. The colored solid squares represent the average step size and error bar indicates the standard deviation (S.D.). The numbers of observed unfolding events for ΔH_2 are 11, 113, 22, 60, and 16 at 3.4 ± 0.4 pN, 4.0 ± 0.4 pN, 5.0 ± 0.5 pN, 6.2 ± 0.7 pN, and 10.0 ± 1.0 pN, respectively. The numbers of observed unfolding events for ΔH_3 are 236, 30, 54 and 17 at around 4.0 ± 0.4 pN, 5.0 ± 0.5 pN, 6.5 ± 0.7 pN, and 10.0 ± 1.0 pN, respectively. Worm-like chain model was used to fit the data, and the optimal fitting parameters were obtained as follows: for ΔH_2 A= 0.85 ± 0.12 nm, L_c= 53.08 ± 3.81 nm; for ΔH_3, A= 0.83 ± 0.05 nm, L_c= 45.49 ± 1.22 nm (means ± the standard error of the fitting).

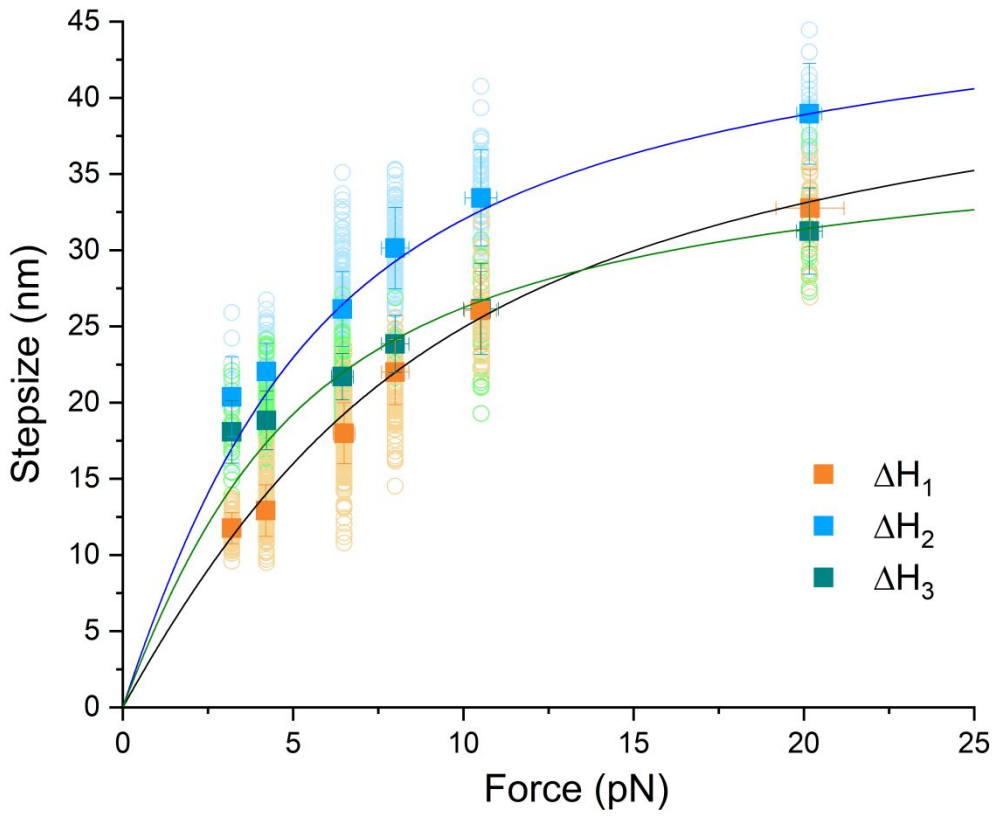

Figure S5. Step sizes of the three jumps of SdrG-Fgβ complex. Step sizes of the three bead height jumps (orange: ΔH_1, blue: ΔH_2, green: ΔH_3) observed in the time traces at different forces collected from more than 30 different tethers. Raw data are presented as light orange, blue or green circles. The colored solid squares denote the average step size and error bar indicates S.D.. The numbers of observed rupture events for ΔH_1 are 64, 134, 257, 186, 54 and 25 at around 3.2 ± 0.4 pN, 4.0 ± 0.4 pN, 6.5 ± 0.7 pN, 8.0 ± 0.8 pN, 10.5 ± 1.1 pN and 20.0 ± 2.0 pN, respectively. The numbers of unfolding events for ΔL_2 are 24, 150, 191, 103, 27, and 23 at 3.2 ± 0.4 pN, 4.0 ± 0.4 pN, 6.5 ± 0.7 pN, 8.0 ± 0.8 pN, 10.5 ± 1.1 pN and 20.0 ± 2.0 pN, respectively. The numbers of unfolding events for ΔH_3 are 15, 77, 273, 186, 57 and 29 at 3.2 ± 0.4 pN, 4.0 ± 0.4 pN, 6.5 ± 0.7 pN, 8.0 ± 0.8 pN, 10.5 ± 1.1 pN and 20.0 ± 2.0 pN, respectively. Worm-like chain model was used to fit the data, and the optimal fitting parameters were obtained as follows: for ΔH_1, A= 0.48 ± 0.05 nm, L_c= 51.56 ± 2.86 nm; for ΔH_2 A = 0.76 ± 0.05 nm, L_c= 53.71 ± 1.36 nm; for ΔH_3, A = 0.85 ± 0.06 nm, L_c= 42.5 ± 0.62 nm (means ± the standard error of the fitting). The latter two steps are consistent with that observed in the SdrG-ΔFgβ (Figure S4), confirming that ΔH_2 and ΔH_3 are corresponded to the unfolding of N3 and N2 domain. Considering an average contour length of 0.36 nm[4] per amino acid, the number of the amino acids involved in the released peptides of the three jumps are about 143, 149, and 118 (a.a.), respectively.

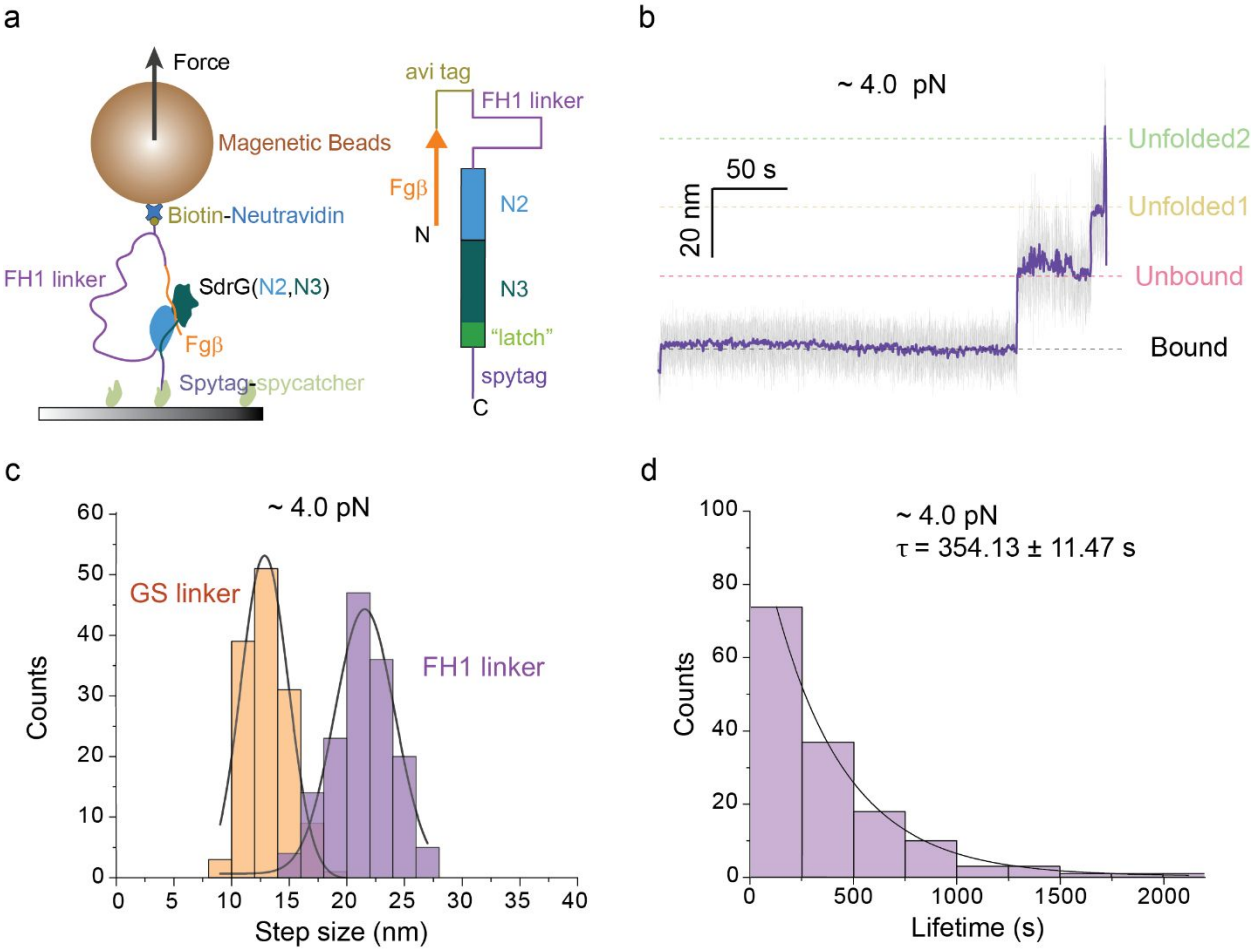

Figure S6. Mechanical response of the SdrG-Fgβ construct with FH1 linker (SdrG-FH1-Fgβ). (a) Left panel: the schematic diagram of single-molecule magnetic tweezer experiment on the SdrG-Fgβ protein construct with FH1 linker (182 a.a., purple). Right panel: schematic illustrating the design of SdrG-FH1-Fgβ construct where the GS-linker (155 a.a.) was replaced by a FH1 linker. (b) Representative bead height-time trace of SdrG-FH1-Fgβ at a constant force of 4.0 ± 0.4 pN. Raw data and smoothed data using FFT with 50 points of window are indicated by gray and purple, respectively. (c) The step size distribution of the dissociation of the SdrG-Fgβ complex with GS linker (orange, n=155) or FH1 linker (purple, n=213) at 4.0 ± 0.4 pN. Through Gaussian fitting of the distributions, the average step size at 4.0 ± 0.4 pN of the dissociation of the complex is: for GS linker, ΔL_1=12.87 ± 0.13 nm; for FH1 linker, ΔL_1=21.55 ± 0.18 nm. The persistence length of FH1 linker A = 0.8 nm was characterized in the previous work[5], indicating a stiffer linker compared to the GS linker (A = 0.48 shown in Figure S5). The contour length of the dissociation of SdrG-FH1-Fgβ can be predicted by using worm-like chain model: L_c = 56.7 nm. (d) Lifetime histogram of SdrG-FH1-Fgβ complex at 4.0 ± 0.4 pN. The total rupture events number is 149, obtained from six independent tethered molecules in multiple single-molecule experiments. A single-exponential decay function was used to fit the distribution (black curve) to get an average lifetime τ = 354.13 ± 11.47 s (means ± the standard error of the fitting).

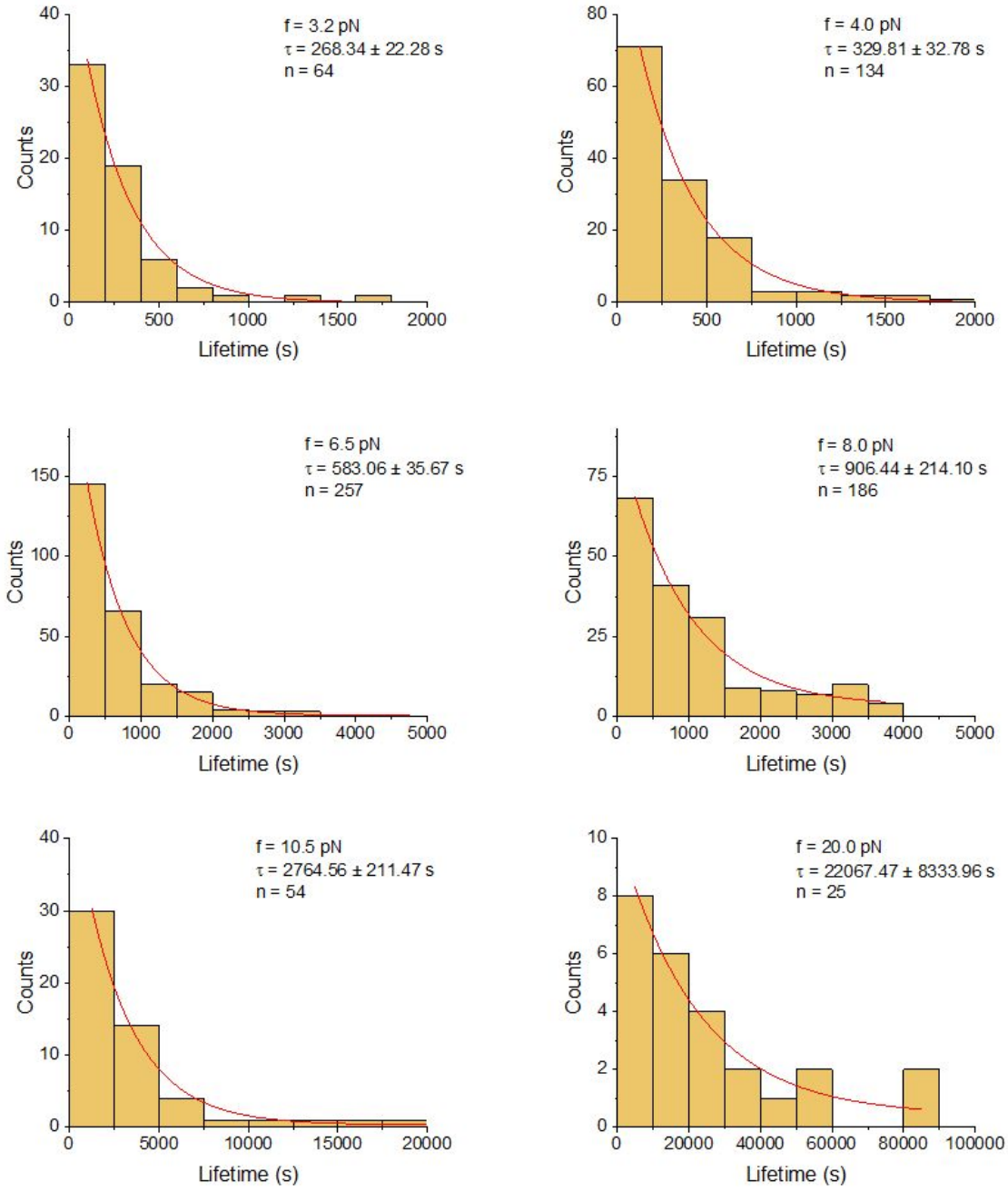

Figure S7. Lifetime histograms of SdrG-Fgβ complex in the force range from 3.2 ± 0.4 pN to 20.0 ± 2.0 pN at 23 °C. Exponential decay ($y(t) = B * \exp(-t/\tau)$) was used to fit each of the distribution (red curves) to obtain an average lifetime τ at different forces. The applied average constant force (f), the average lifetime (τ), and number of the collected rupture events (n) at each force are shown in the figure (means ± the standard error of the fitting).

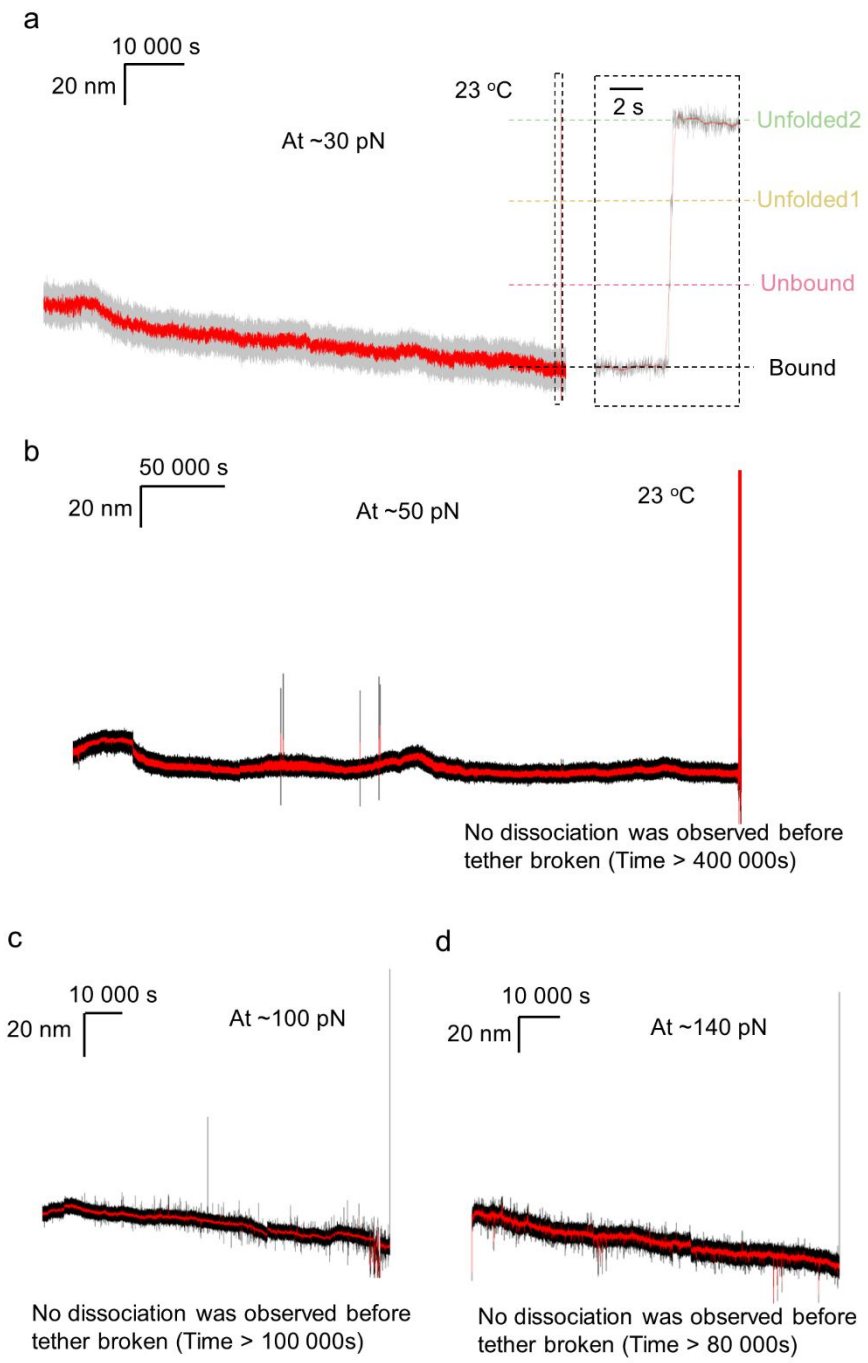

Figure S8. Representative bead height-time traces under constant force of 30 ± 3.0 pN and 50 ± 5.0 pN. (a) Representative bead height-time trace of the protein construct containing SdrG-Fgβ complex at 30 ± 3.0 pN. Three stepwise jumps corresponding to the transitions of the dissociation of SdrG-Fgβ complex (from bound to unbound state), and two unfolding of the N2, N3 domain of SdrG. Right panel is the enlarged time trace around the step jumping transitions. The average lifetime at this force is calculated to be 124 486.4 ± 70 963.5 s from four independent molecules. mean ± S.D.. (b) Representative bead height-time trace of SdrG-Fgβ complex at 50 ± 5.0 pN. No dissociation was observed before the tether was broken after more than 400 000 s.

Similar results were observed from more than five tethers, where the tethers were broken after 150 000 – 500 000 s due to the rupture of the other part of the tether. (c) Representative bead height-time trace of SdrG-Fgβ complex at 100.0 ± 10.0 pN and (d) at 140.0 ± 14.0 pN . Under both forces, no dissociation events were observed before the tethers were broken due to the rupture of the other part of the tether after long duration. Similar results were repeated for more than five tethers, respectively. Raw data and smoothed data using FFT with 50 points of window are indicated by gray/black and red, respectively.

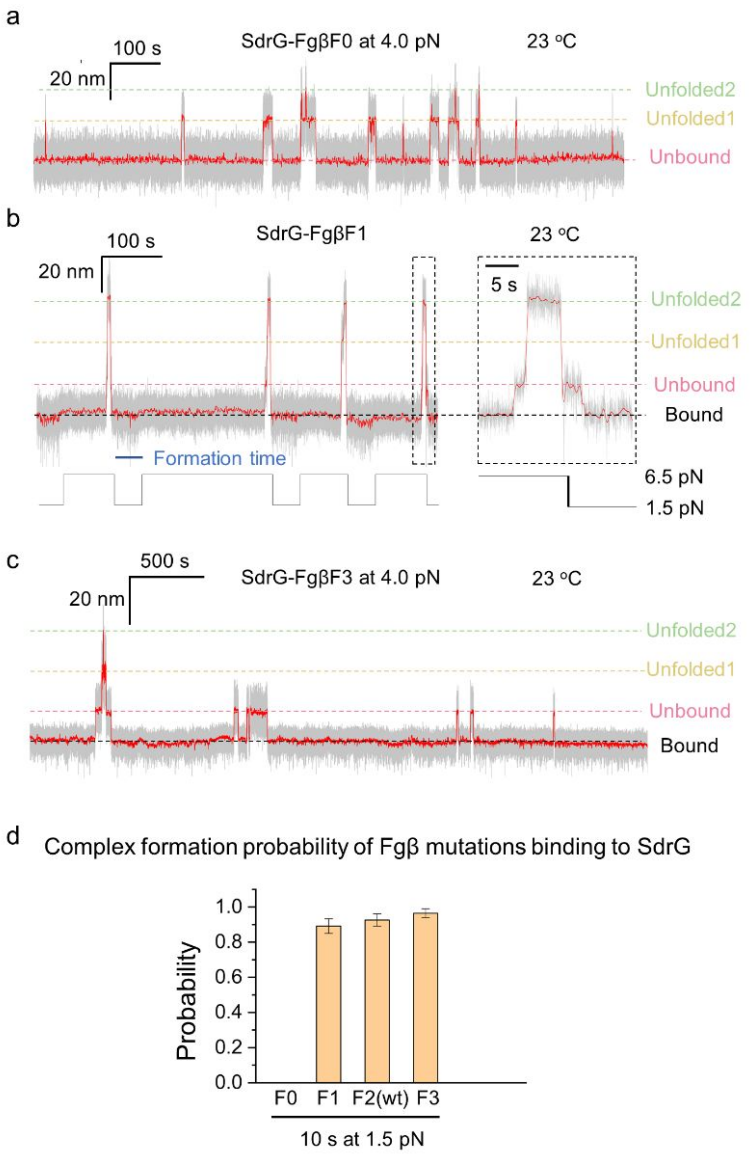

Figure S9. Mechanical responses of SdrG-FgβF0, SdrG-FgβF1, and SdrG-FgβF3. (a) Representative bead height-time trace of SdrG-FgβF0 complex at 4.0 ± 0,4 pN at 23 °C. Two step jumps corresponding to the unfolding of the N2, N3 domain was obtained. Similar two step jumps were observed in all of the tested molecules (n > 5), while no dissociation signal was obtained with our time resolution (200 Hz). (b) Representative bead height-time trace of SdrG-FgβF1 complex under force-jumping cycles between 6.5 ± 0.7 pN and 1.5 ± 0.2 pN. The three stepwise jumps corresponding to the transitions of the dissociation of the complex (from bound to unbound state), and two unfolding of the N2, N3 domain of SdrG. Right panel is the enlarged time trace around the step jumping transitions and formation of the complex when force jumped back to 1.5 ± 0.2 pN. (c) Representative bead height-time trace of SdrG-FgβF3 complex at around 4.0 pN at 23 °C. Raw data and smoothed data using FFT with 50 points of window are indicated by gray and red, respectively. (d) Comparison of the complex formation probabilities of different Fgβ mutations binding to SdrG after waiting times of 10 s at 1.5 ± 0.2 pN, respectively. Error bar indicate mean ± S. D.

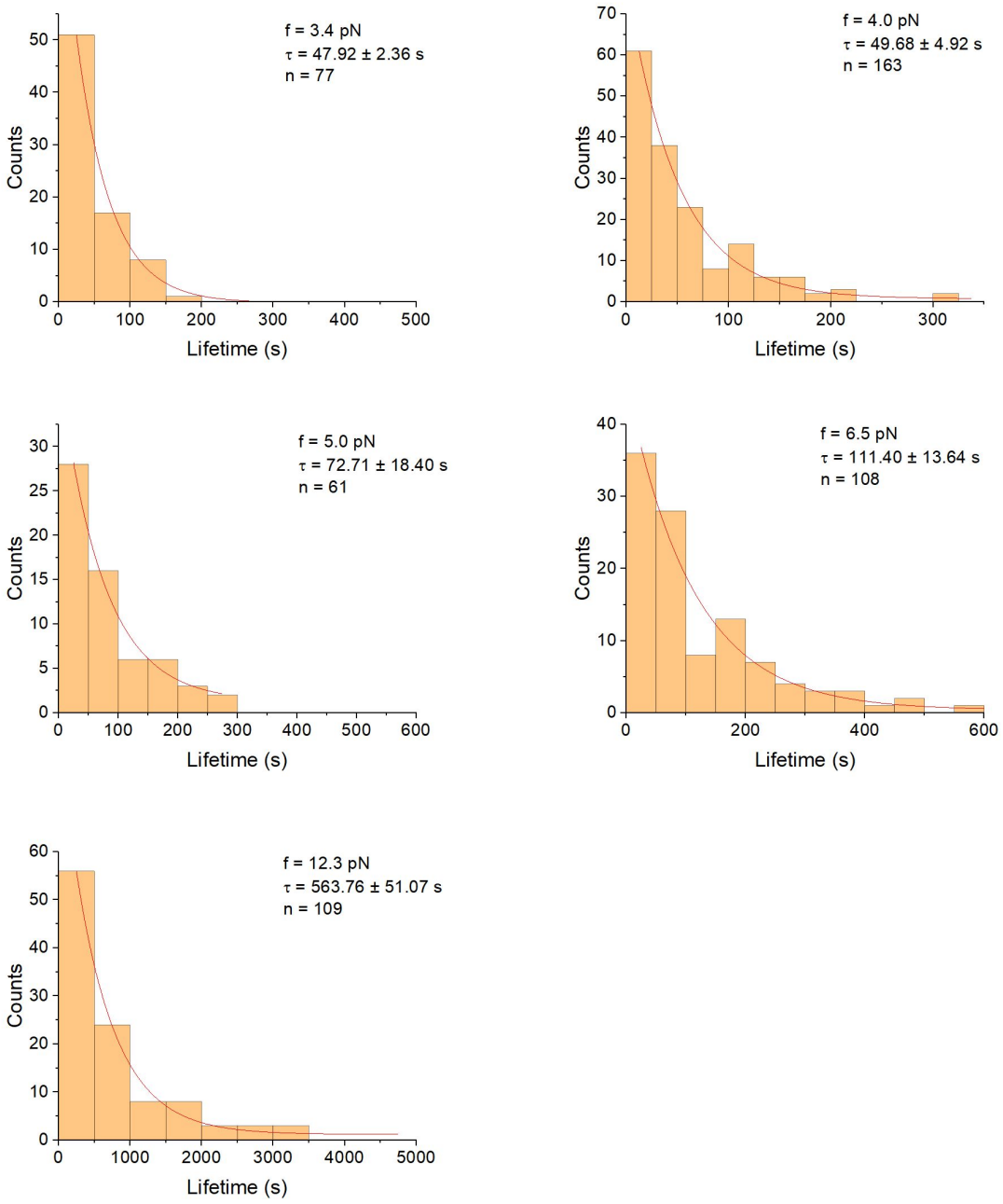

Figure S10. Lifetime histograms of SdrG-FgβF1 complex in the force range from 3.4 ± 0.4 pN to 12.3 ± 1.3 pN at 23 ºC. The lifetimes at different forces are collected from five different tethers. Exponential decay function was used to fit each of the distribution (red curves) to obtain an average lifetime τ at different forces. The applied average constant force (f), the average lifetime (τ), and number of the collected rupture events (n) at each force are shown in the figure.

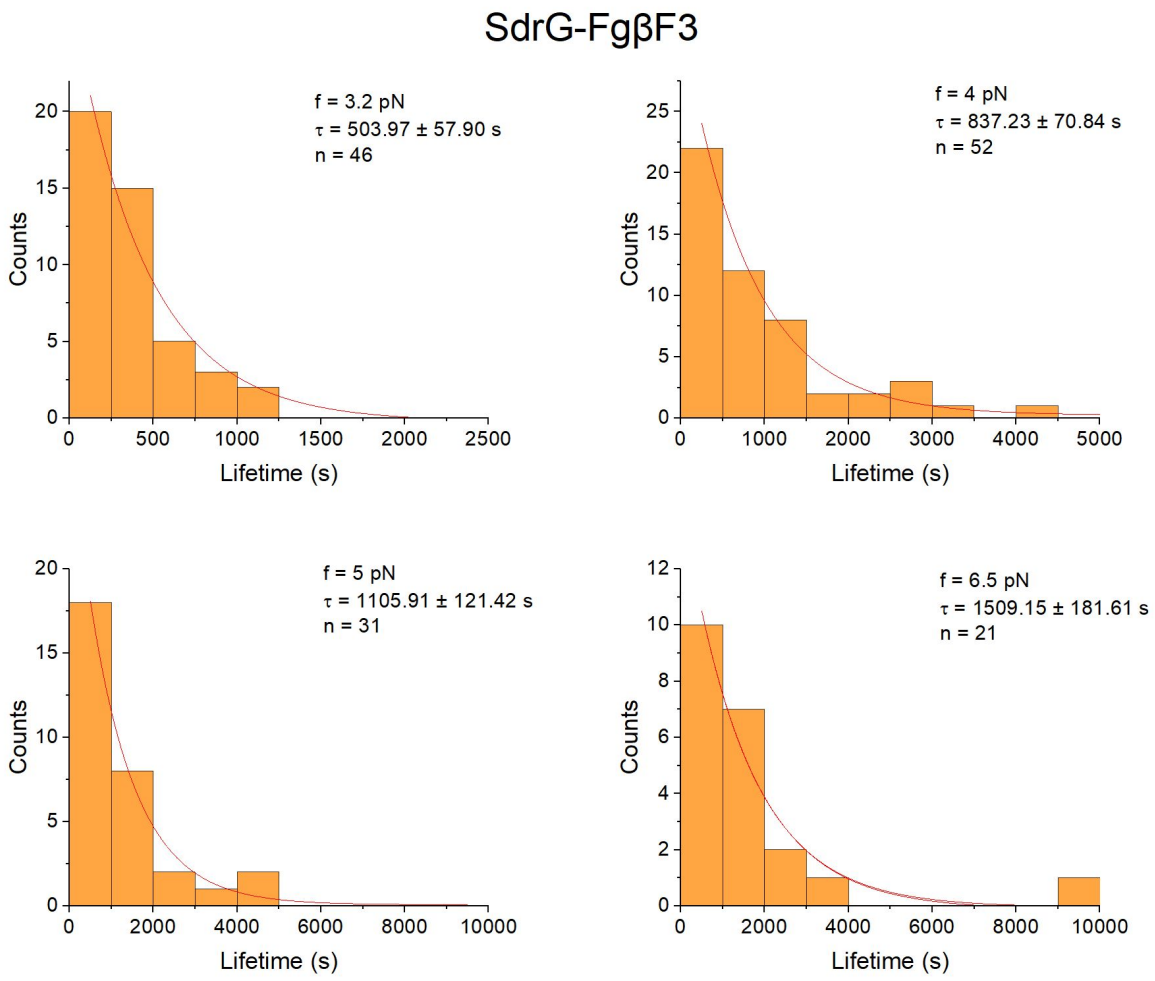

Figure S11. Lifetime histograms of SdrG-FgβF3 complex in the force range from 3.2 ± 0.4 pN to 6.5 ± 0.7 pN at 23 ºC. The lifetimes at different forces are collected from 14 different tethers. Exponential decay function was used to fit each of the distribution (red curves) to obtain an average lifetime τ at different forces. The applied average constant force (f), the average lifetime (τ), and number of the collected rupture events (n) at each force are shown in the figure.

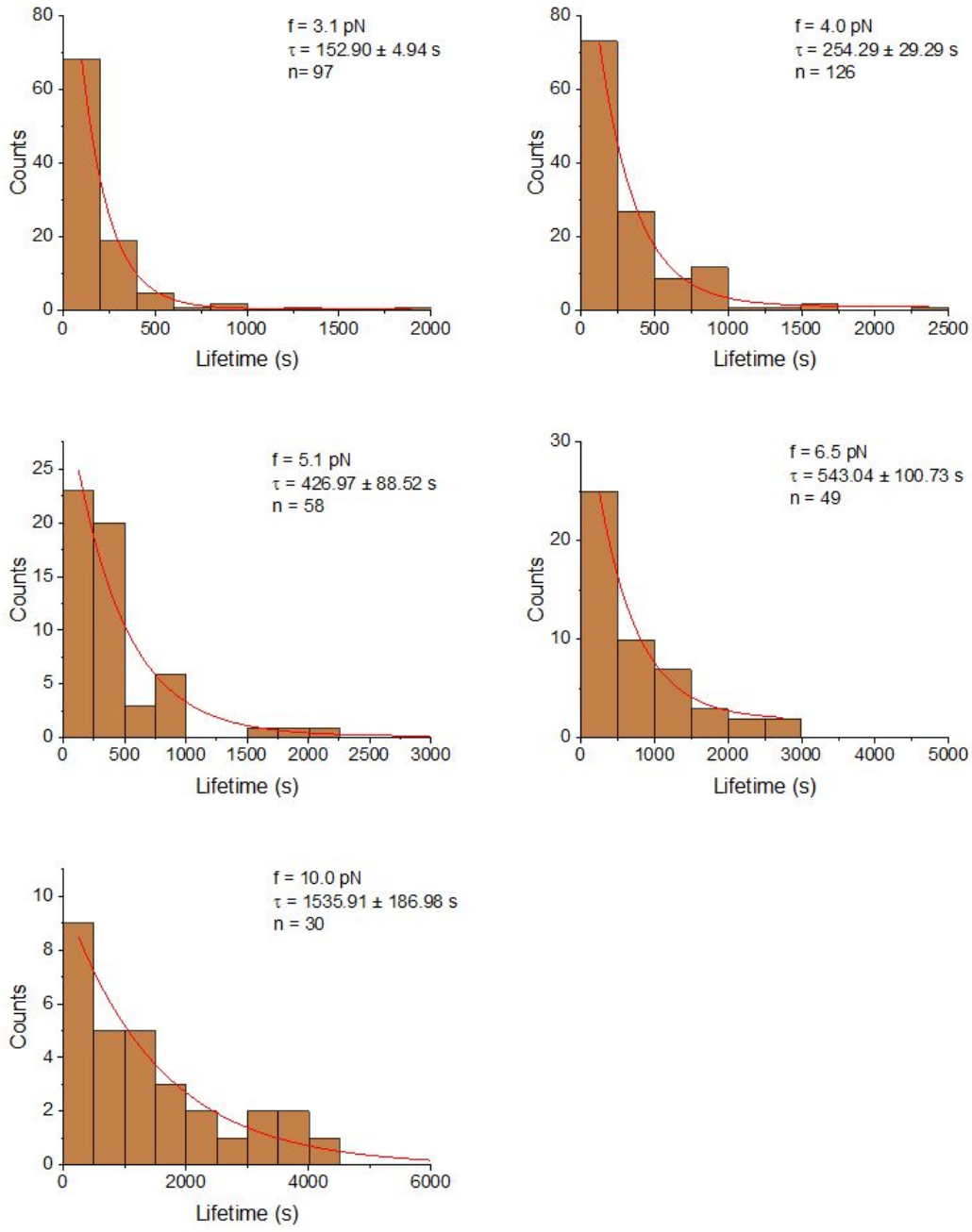

Figure S12. Lifetime histograms of SdrG-FgβFFSARG complex in the force range from 3.1 ± 0.4 pN to 10.0 ± 1.0 pN at 23 ºC. The ligand was truncated to remain the minimal six residue (FFSARG) that was sufficient for the binding. The lifetimes at different forces are collected from five different tethers. Exponential decay function was used to fit each of the distribution (red curves) to obtain an average lifetime $\boldsymbol{\tau}$ at different forces. The applied average constant force (f), the average lifetime (τ), and number of the collected rupture events (n) from at each force are shown in the figure.

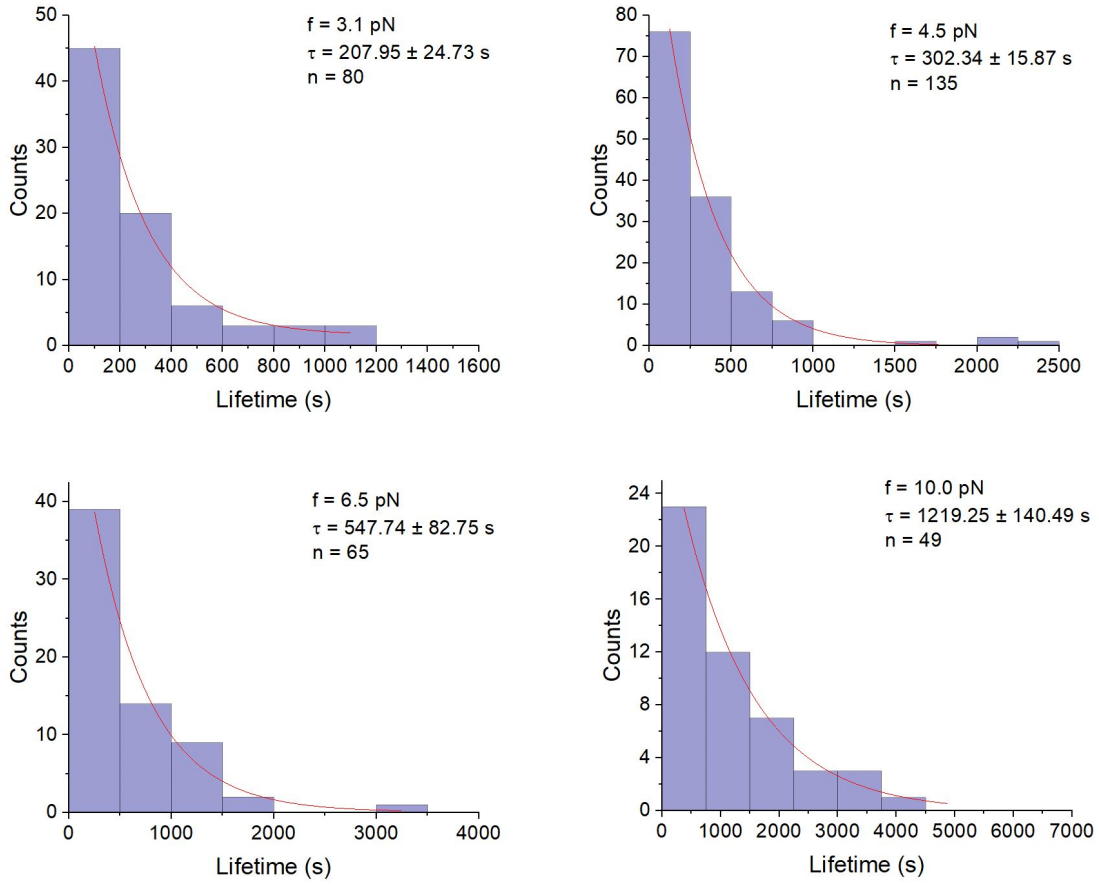

Figure S13. Lifetime histograms of SdrG-FgβdN4 complex in the force range from 3.1 ± 0.4 pN to 10.0 ± 1.0 pN at 23 °C. The four amino acids (NEEG) in the N terminus of the ligand were truncated. The lifetimes at different forces are collected from 6 different tethers. Exponential decay function was used to fit each of the distribution (red curves) to obtain an average lifetime τ at different forces. The applied average constant force (f), the average lifetime (τ), and number of the collected rupture events (n) at each force are shown in the figure.

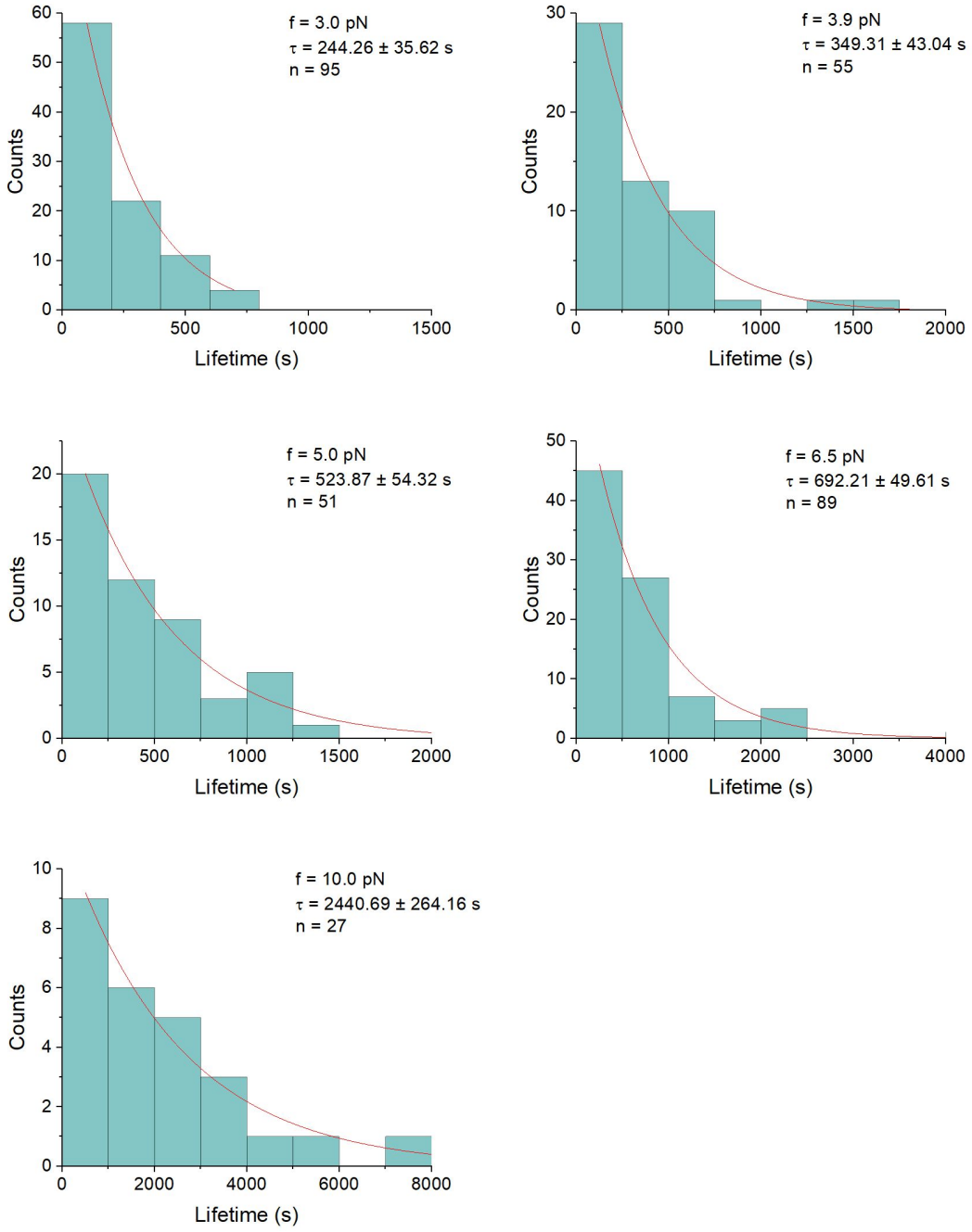

Figure S14. Lifetime histograms of SdrG-FgβdC5 complex in the force range from 3.1 ± 0.4 pN to 10.0 ± 1.0 pN at 23 °C. The five amino acids (HRPLD) in the C-terminus of the ligand were truncated. The lifetimes at different forces are collected from 10 different tethers. Exponential decay function was used to fit each of the distribution (red curves) to obtain an average lifetime τ at different forces. The applied average constant force (f), the average lifetime (τ), and number of the collected rupture events (n) at each force are shown in the figure.

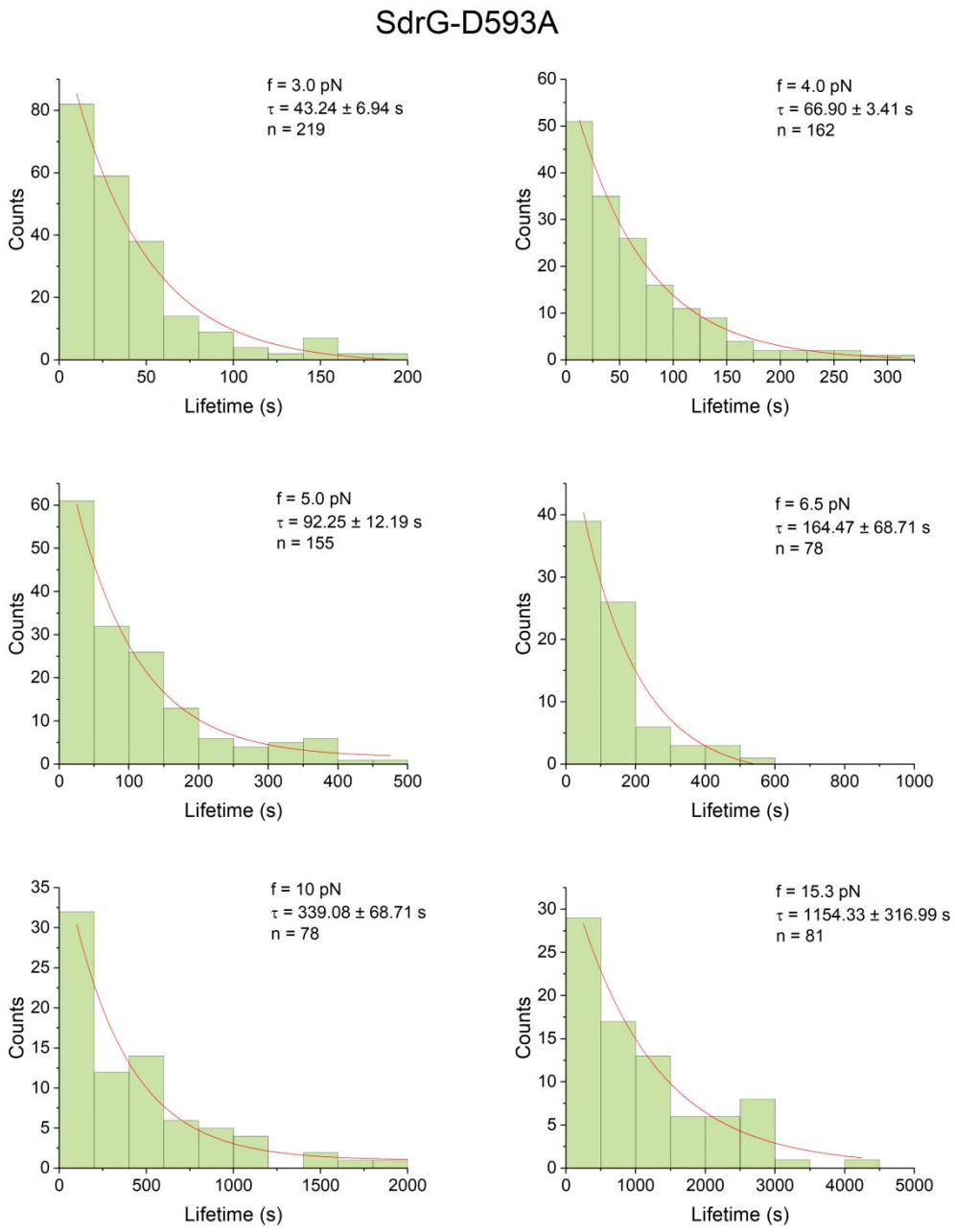

Figure S15. Lifetime histograms of D593A protein construct (SdrG_D593A-Fgβ) in the force range from 3.0 ± 0.3 pN to 15.3 ± 1.6 pN at 23 ºC. The lifetimes at different forces are collected from 7 different tethers. Exponential decay function was used to fit each of the distribution (red curves) to obtain an average lifetime τ at different forces. The applied average constant force (f), the average lifetime (τ), and number of the collected rupture events (n) at each force are shown in the figure.

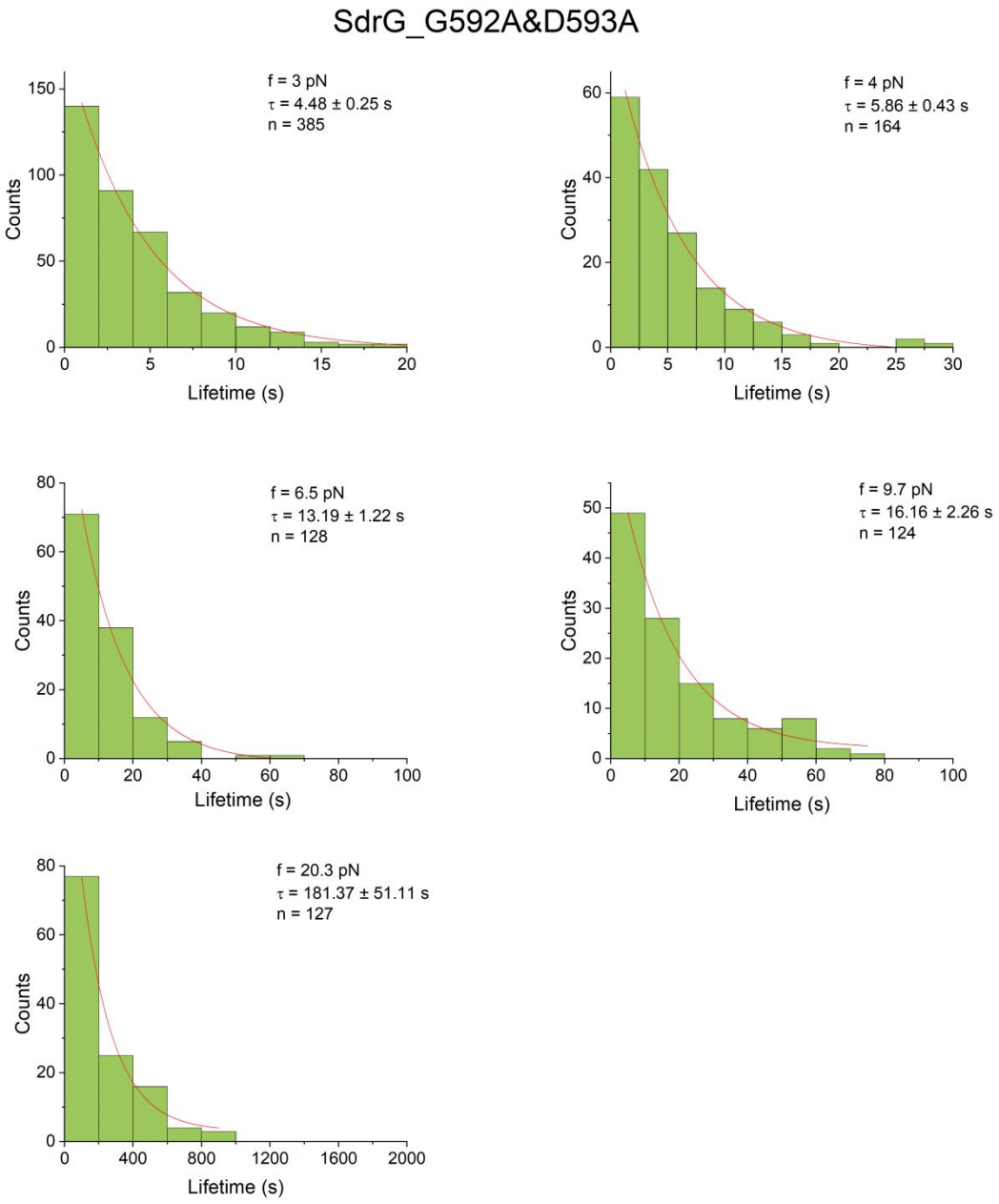

Figure S16. Lifetime histograms of the G592A+D593A construct (SdrG_G592A+D593A-Fgβ) in the force range from 3.0 ± 0.3 pN to 20.3 ± 2.1 pN at 23 °C. The lifetimes at different forces are collected from five different tethers. Exponential decay function was used to fit each of the distribution (red curves) to obtain an average lifetime τ at different forces. The applied average constant force (f), the average lifetime (τ), and number of the collected rupture events (n) at each force are shown in the figure.

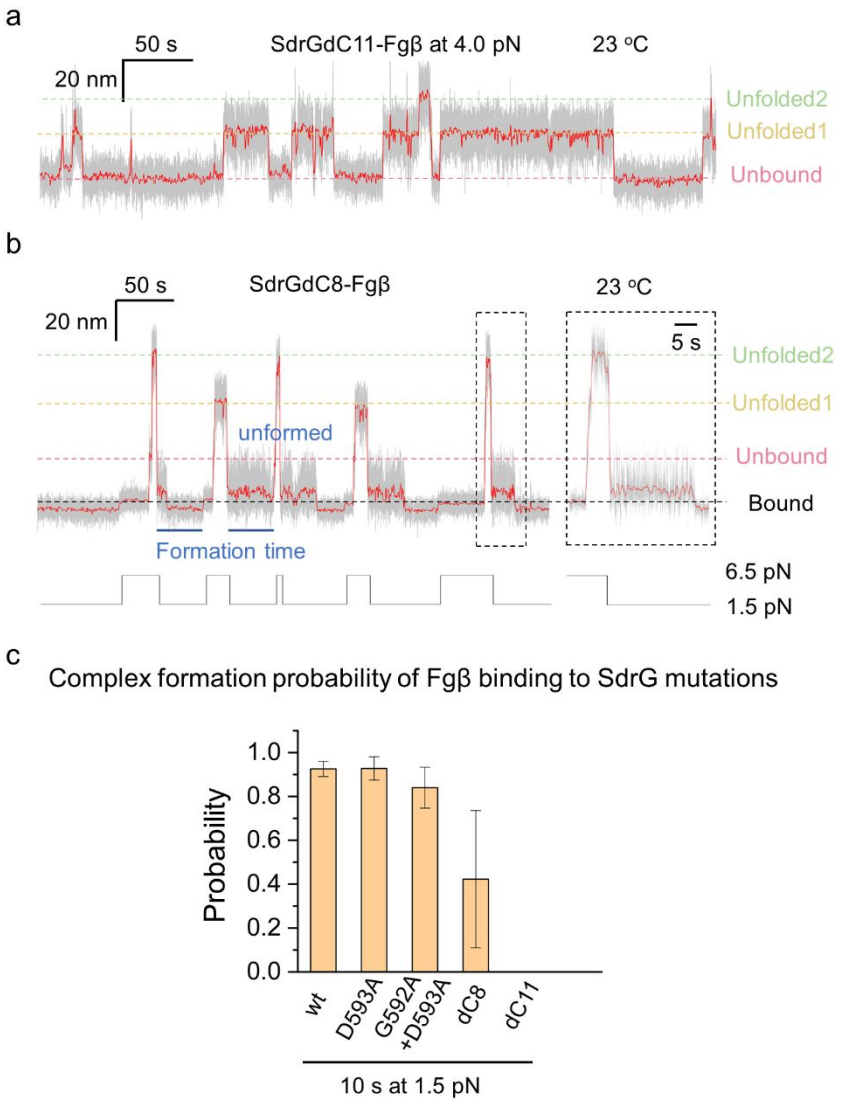

Figure S17. Mechanical responses of the SdrG truncations with wild-type Fgβ (SdrG_dC11-Fgβ, and SdrG_dC8-Fgβ). (a) Representative bead height-time trace of SdrG_dC11-Fgβ complex at 4.0 ± 0.4 pN at 23 °C. Two step jumps corresponding to the unfolding of the N2, N3 domain was obtained. Similar two step jumps were observed in all tested molecules ($n > 5$), while no dissociation signal was obtained with our time resolution (200 Hz). (b) Representative bead height-time trace of SdrG_dC8-Fgβ complex under force-jumping cycles between 6.5 ± 0.7 pN and 1.5 ± 0.2 pN. The three stepwise jumps corresponding to the transitions of the dissociation of the complex (from bound to unbound state), and two unfolding of the N2, N3 domain of SdrG. Right panel is the enlarged time trace around the step jumping transitions and formation of the complex when force jumped back to 1.5 ± 0.2 pN. Raw data and smoothed data using FFT with 50 points of window are indicated by gray and red, respectively. (c) Comparison of the complex formation probabilities of Fgβ binding to SdrG with mutated or truncated "latch" strand after waiting times of 10 s at 1.5 ± 0.2 pN, respectively. Error bars indicate mean ± S. D..

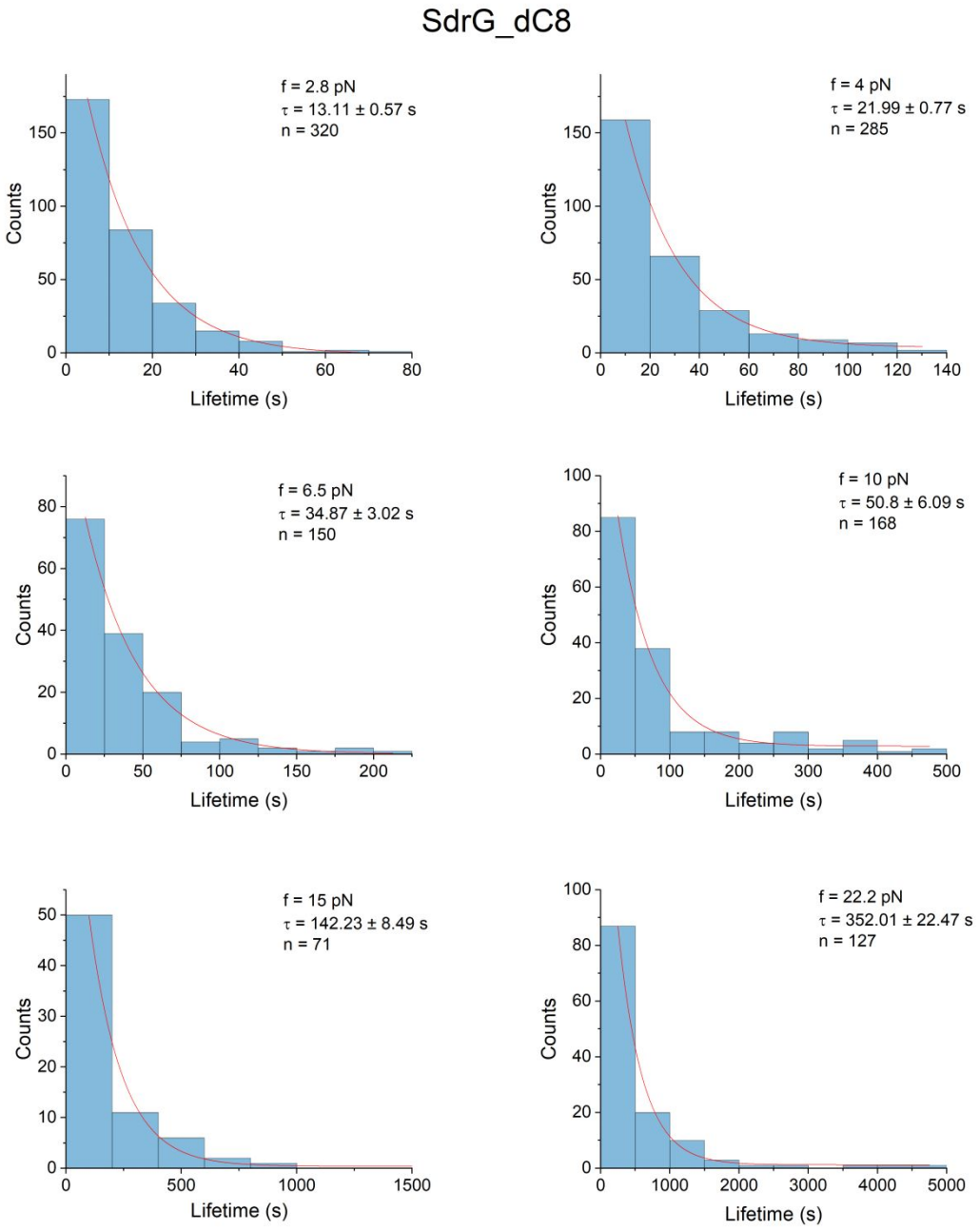

Figure S18. Lifetime histograms of SdrG_dC8-Fgβ complex in the force range from 2.8 ± 0.3 pN to 22.2 ± 2.3 pN at 23 °C. The lifetimes at different forces are collected from 27 different tethers. Exponential decay function was used to fit each of the distribution (red curves) to obtain an average lifetime τ at different forces. The applied average constant force (f), the average lifetime (τ), and number of the collected rupture events (n) at each force are shown in the figure.

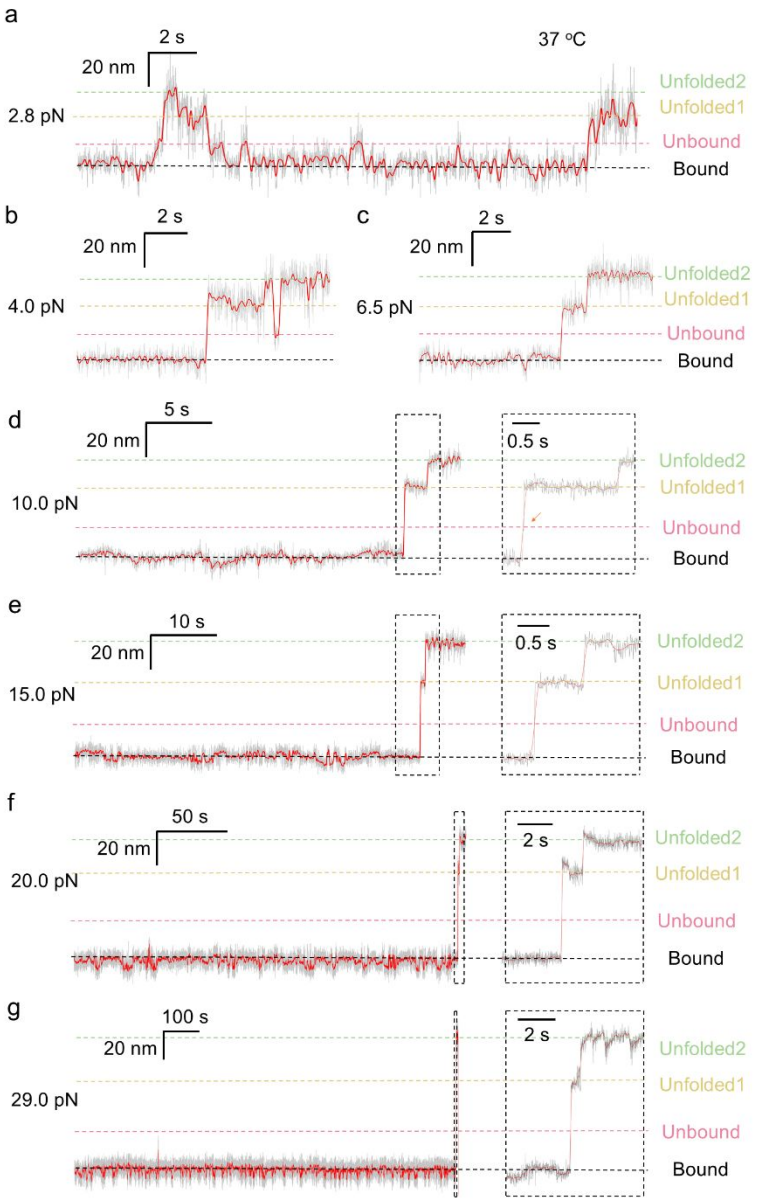

Figure S19. Representative bead height-time traces of protein construct containing wild-type SdrG-Fgβ complex under force range from 2.6 ± 0.3 pN to 30.0 ± 3.0 pN at 37 °C. Representative bead height-time traces of SdrG-Fgβ complex at around (a) 2.8 ± 0.3 pN, (b) 4.0 ± 0.4 pN, (c) 6.5 ± 0.7 pN, (d) 10.0 ± 1.0 pN, (e) 15.0 ± 1.5 pN, (f) 20.0 ± 2.0 pN, and (g) 29.0 ± 2.9 pN are shown with three stepwise jumps corresponding to the transitions of the dissociation of SdrG-Fgβ complex (from bound to unbound state), and two unfolding of the N2, N3 domain of SdrG. Right panels of (e)−(g) are the enlarged time traces around the step jumping transitions. Raw data and smoothed data using FFT with 10 points of window are indicated by gray and red, respectively.

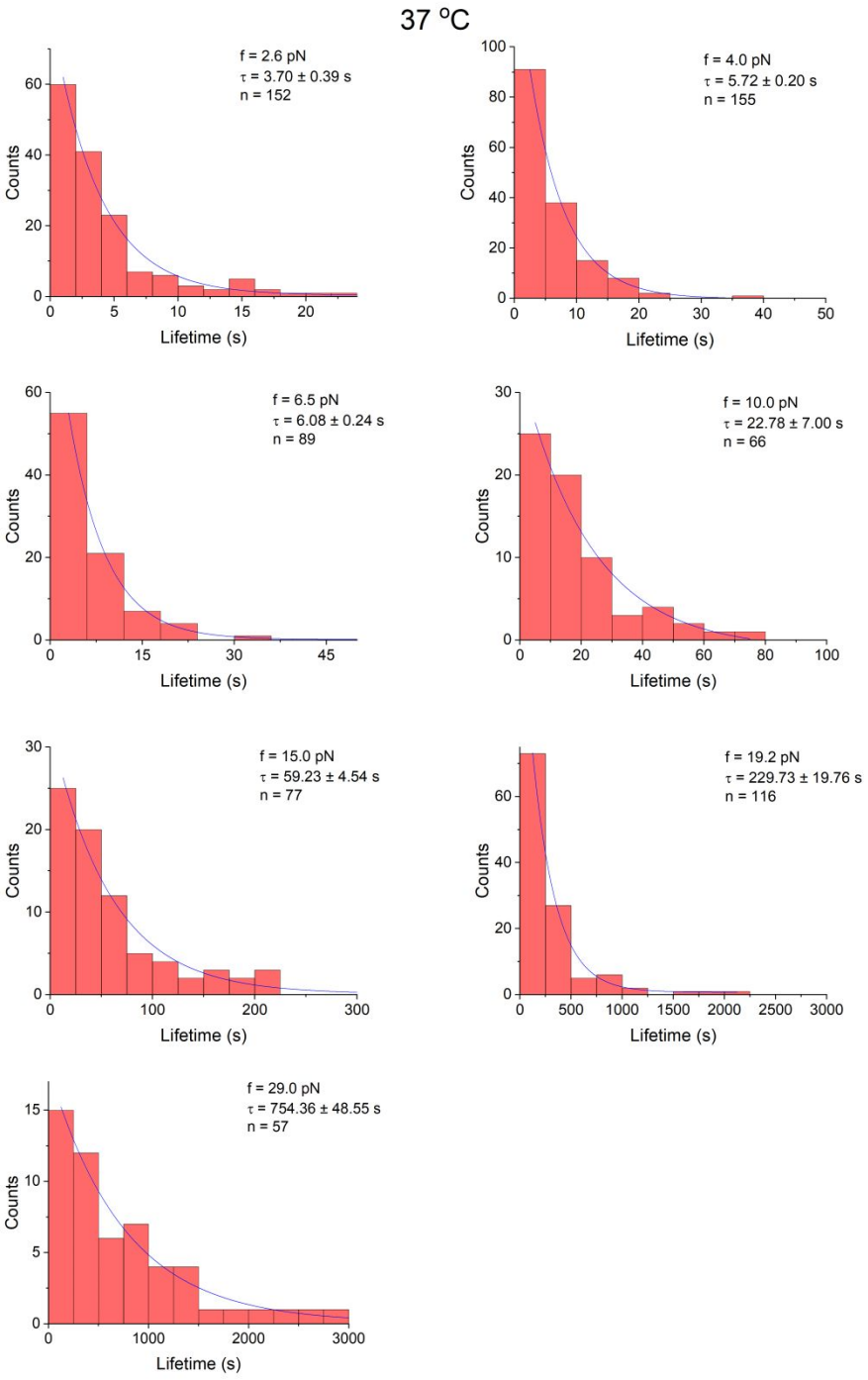

Figure S20. Lifetime histograms of SdrG-Fgβ complex in the force range from 2.6 ± 0.3 pN to 29.0 ± 2.9 pN at 37 °C. The lifetimes at different forces are collected from > five different tethers. Exponential decay function was used to fit each of the distribution (blue curves) to obtain an average lifetime τ at different forces. The applied average constant force (f), the average lifetime (τ), and number of the collected rupture events (n) at each force are shown in the figure.

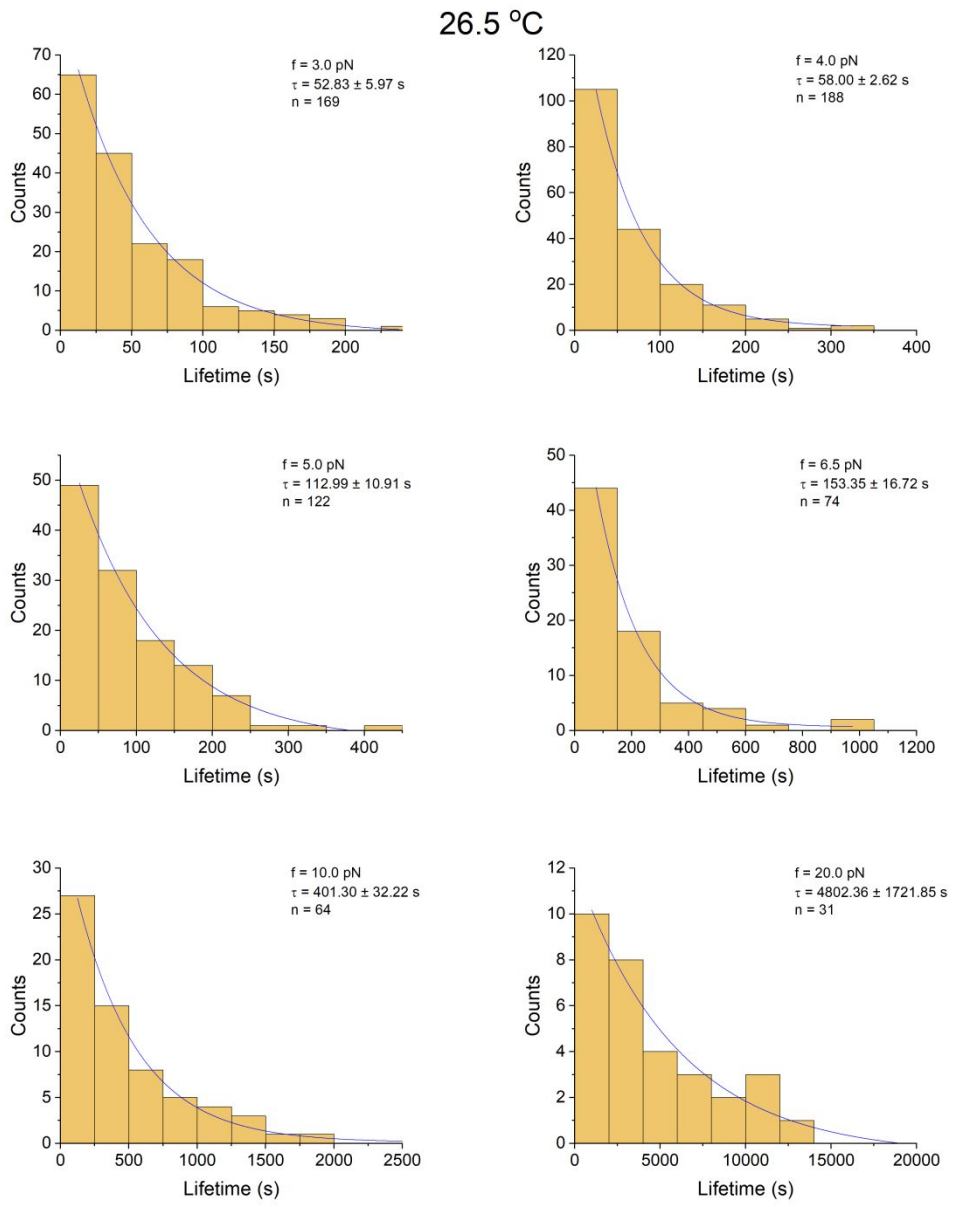

Figure S21. Lifetime histograms of SdrG-Fgβ complex in the force range from 3.0 ± 0.3 pN to 20.0 ± 2.0 pN at 26.5 °C. The lifetimes at different forces are collected from six different tethers. Exponential decay function was used to fit each of the distribution (blue curves) to obtain an average lifetime τ at different forces. The applied average constant force (*f*), the average lifetime (τ), and number of the collected rupture events (*n*) at each force are shown in the figure.

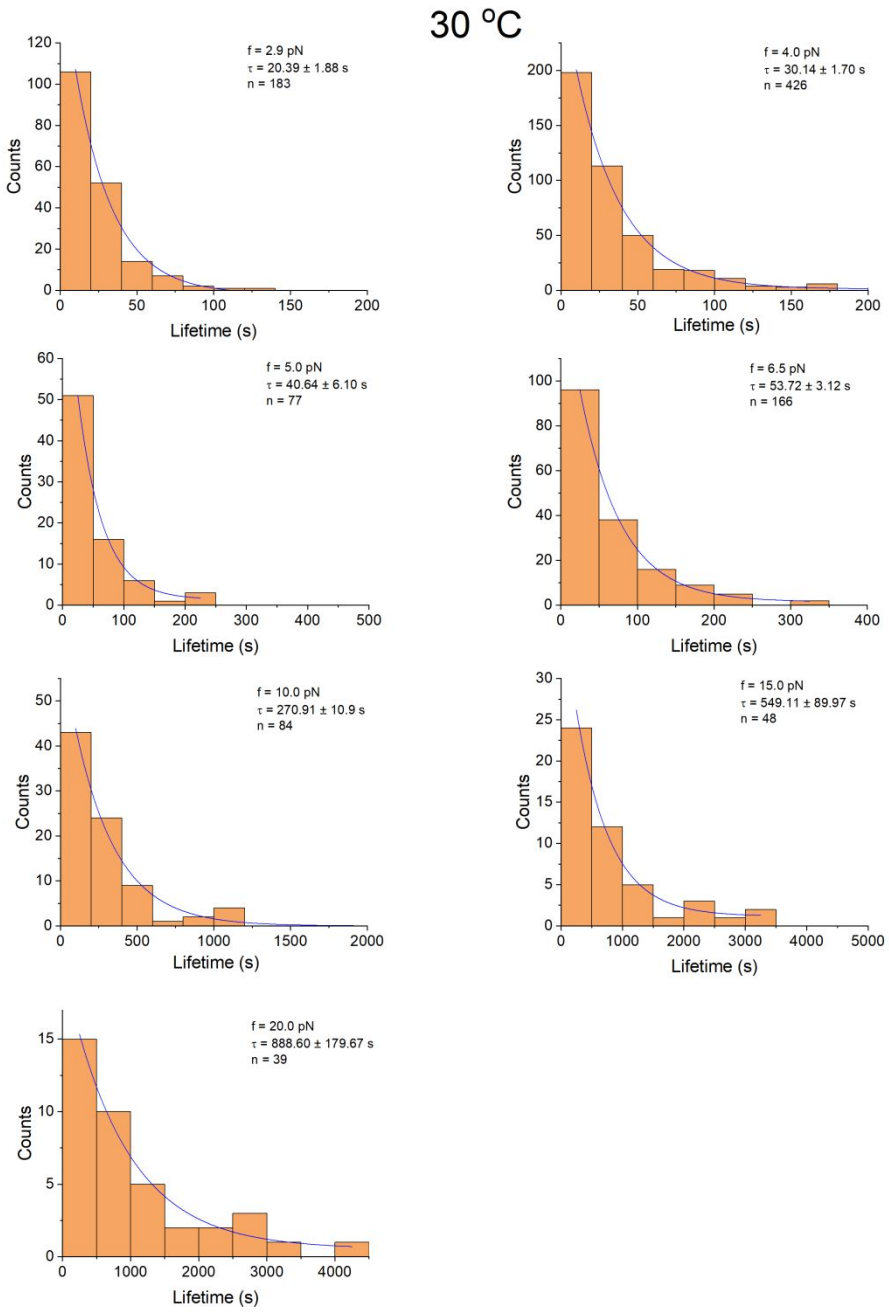

Figure S22. Lifetime histograms of SdrG-Fgβ complex in the force range from 2.9 ± 0.3 pN to 20.0 ± 2.0 pN at 30 °C. The lifetimes at different forces are collected from five different tethers. Exponential decay function was used to fit each of the distribution (blue curves) to obtain an average lifetime τ at different forces. The applied average constant force (*f*), the average lifetime (τ), and number of the collected rupture events (*n*) at each force are shown in the figure.

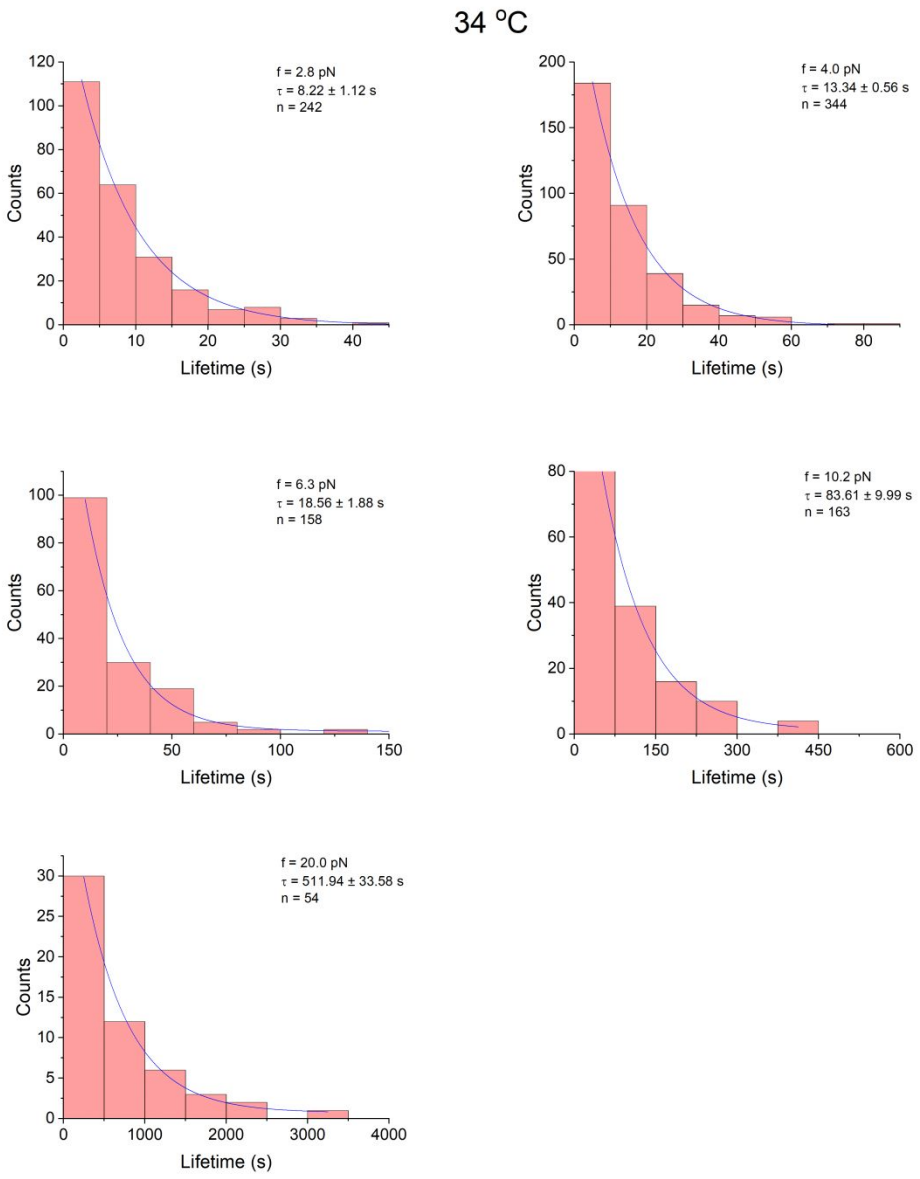

Figure S23. Lifetime histograms of SdrG-Fgβ complex in the force range from 2.8 ± 0.3 pN to 20.0 ± 2.0 pN at 34 °C. The lifetimes at different forces are collected from 13 different tethers. Exponential decay function was used to fit each of the distribution (blue curves) to obtain an average lifetime τ at different forces. The applied average constant force (*f*), the average lifetime (τ), and number of the collected rupture events (*n*) at each force are shown in the figure.

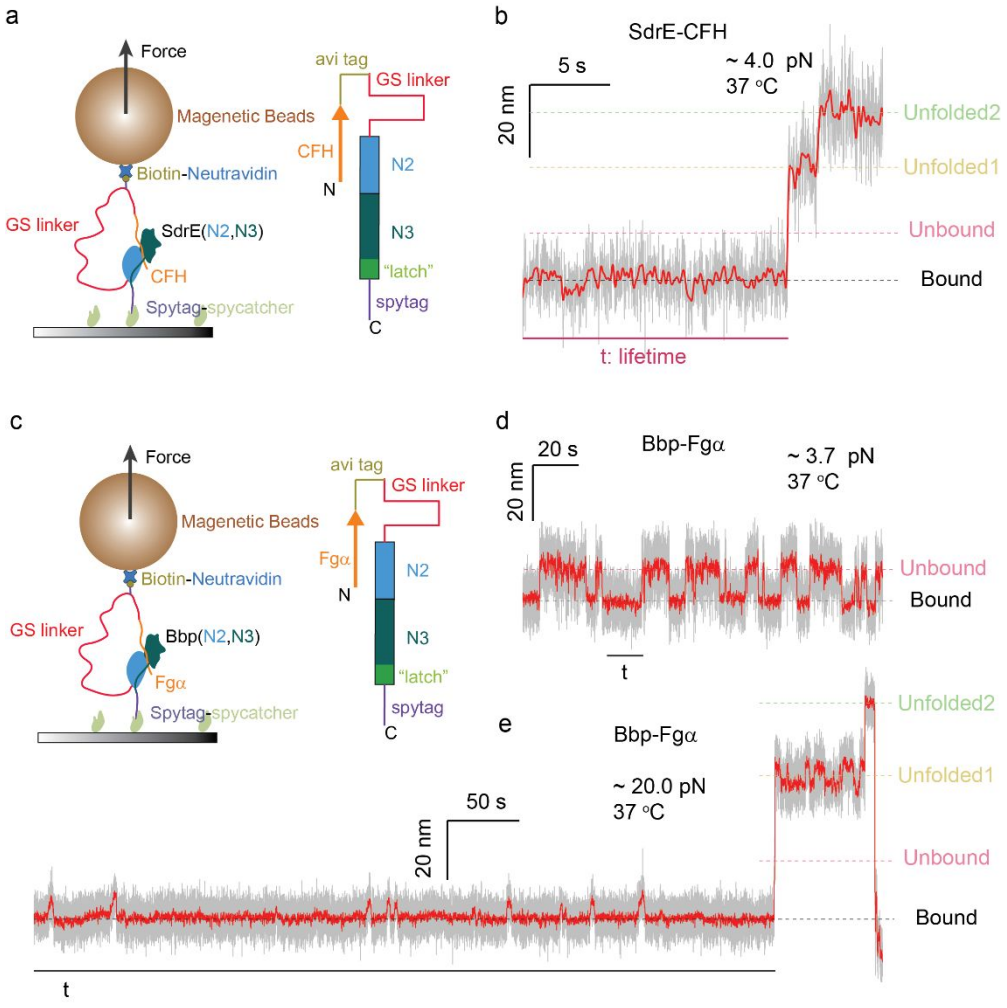

Figure S24. Mechanical signatures of SdrE-CFH and Bbp-Fgα at 37 °C. (a) Left panel: schematic diagram of single-molecule magnetic tweezer experiment with SdrE-CFH construct. Right panel: schematic illustrating the design of SdrE-CFH construct ensuring the native pulling geometry from both C-terminus of the SdrE and CFH. (b) Representative bead height-time trace of SdrE-CFH complex at 4.0 ± 0.4 pN at 37 °C. (c) Left panel: schematic diagram of single-molecule magnetic tweezer experiment Bbp-Fgα construct. Right panel: schematic illustrating the molecular design of Bbp-Fgα construct ensuring the native pulling geometry from both C-terminus of the Bbp and Fgα. (d) Representative bead height-time trace of Bbp-Fgα complex at 3.7 ± 0.4 pN at 37 °C. (e) Representative bead height-time trace of Bbp-Fgα complex at 20.0 ± 2.0 pN at 37 °C, where the three steps correspond to the dissociation of the complex and the unfolding of N2, N3 domain. Raw data and smoothed data using FFT with 10 points of window are indicated by gray and red, respectively.

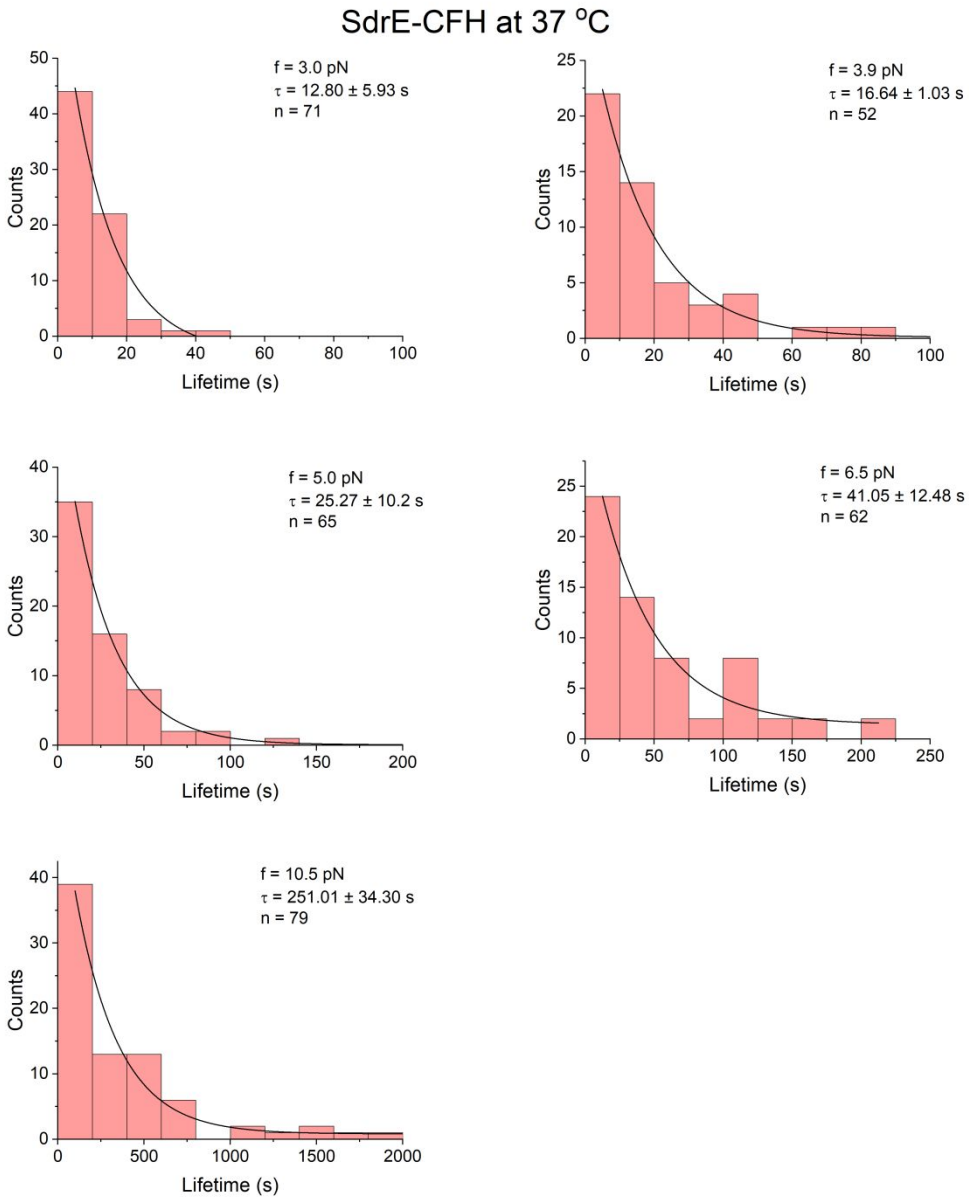

Figure S25. Lifetime histograms of SdrE-CFH complex in the force range from 3.0 ± 0.3 pN to 10.5 ± 1.1 pN at 37 °C. The lifetimes at different forces are collected from 13 different tethers. Exponential decay function was used to fit each of the distribution (black curves) to obtain an average lifetime τ at different forces. The applied average constant force (f), the average lifetime (τ), and number of the collected rupture events (n) at each force are shown in the figure.

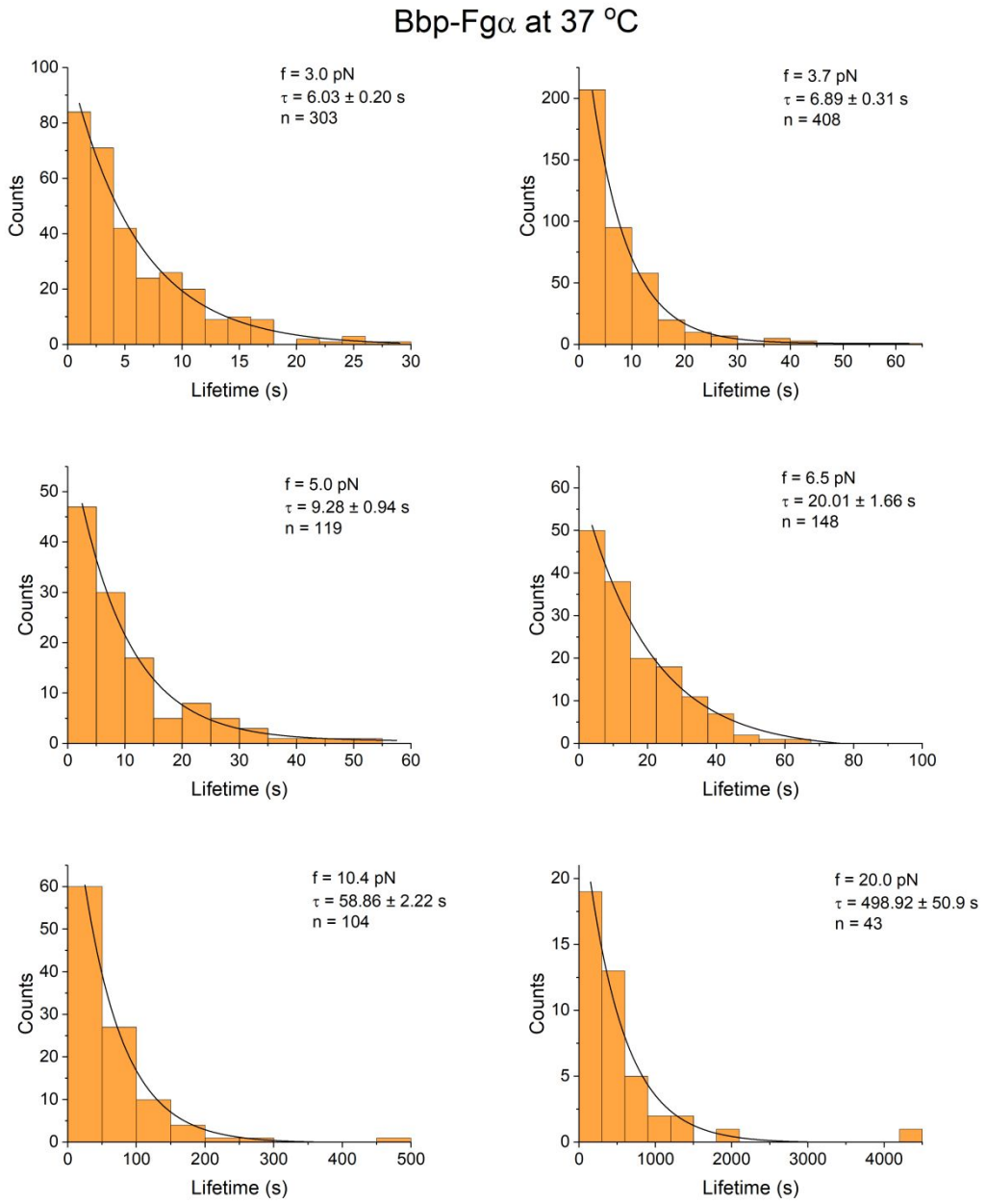

Figure S26. Lifetime histograms of Bbp-Fgα complex in the force range from 3.0 ± 0.3 pN to 20.0 ± 2.0 pN at 37 °C. The lifetimes at different forces are collected from 9 different tethers. Exponential decay function was used to fit each of the distribution (black curves) to obtain an average lifetime τ at different forces. The applied average constant force (f), the average lifetime (τ), and number of the collected rupture events (n) at each force are shown in the figure.

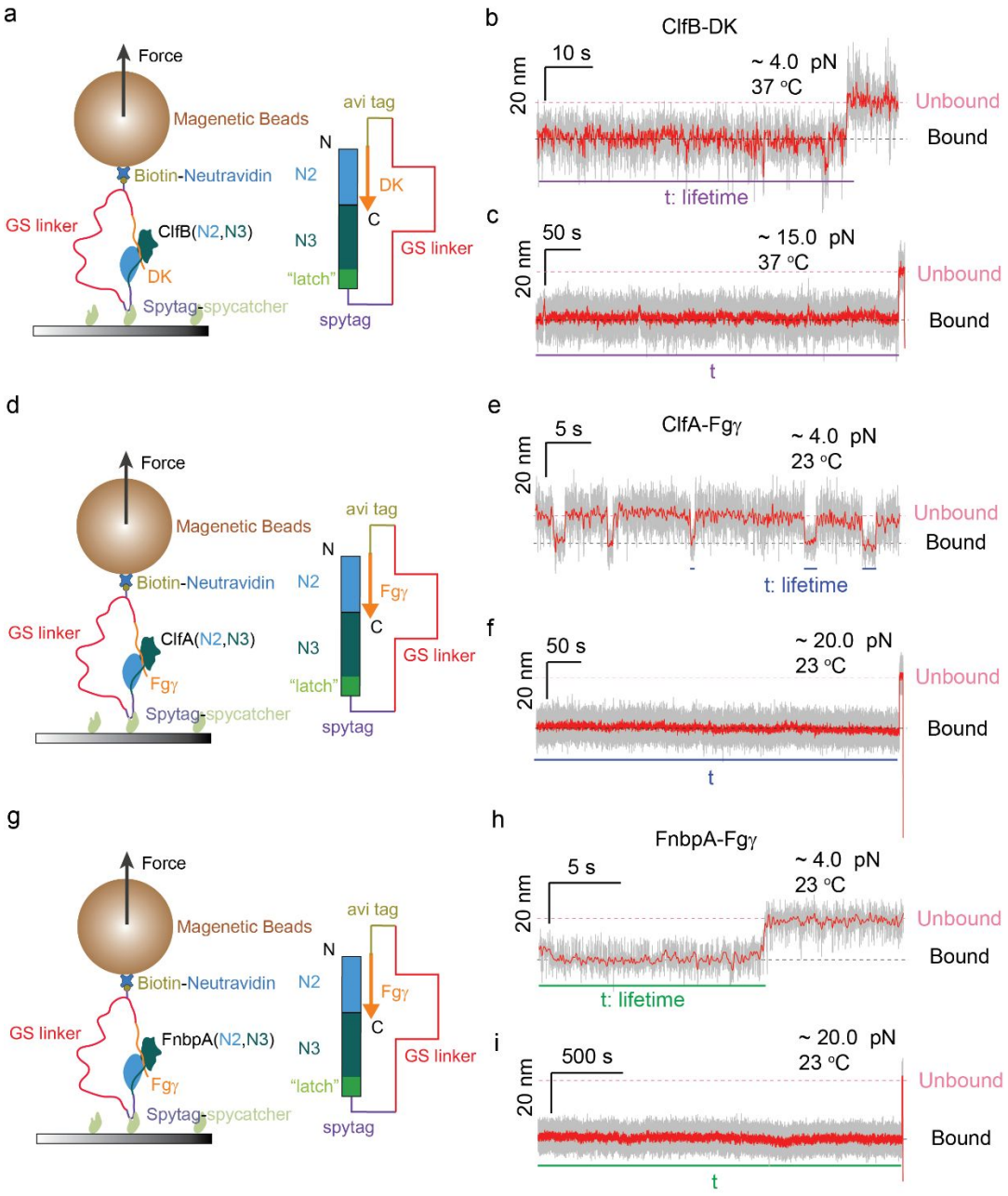

Figure S27. Mechanical signatures of ClfB-DK, ClfA-Fgγ, and FnbpA-Fgγ. (a) Left panel: schematic diagram of single-molecule magnetic-tweezers experiment with ClfB-DK complex. Right panel: schematic illustrating the design of ClfB-DK construct ensuring the native pulling geometry from the C-terminus of ClfB and the N-terminus of DK. (b) Representative bead height-time trace of ClfB-DK complex at 4.0 ± 0.4 pN at 37 °C. (c) Representative bead height-time trace of ClfB-DK complex at 15.0 ± 1.5 pN at 37 °C. (d) Left panel: schematic diagram of single-molecule experiment on the ClfA-Fgγ complex. Right panel: schematic illustrating the design of the ClfA-Fgγ construct ensuring the native pulling geometry from the C-terminus of ClfA and the N-terminus of Fgγ. (e) Representative bead height-time trace of ClfA-Fgγ complex at 4.0 ± 0.4 pN at 23 °C. The dissociation of ClfA-Fgγ at 4.0 ± 0.4 pN was in seconds at 23 °C, which could not

be detected at 37 °C. (f) Representative bead height-time trace of ClfA-Fgγ complex at 20.0 ± 2.0 pN at 23 °C. (g) Left panel: schematic diagram of single-molecule magnetic tweezer experiment FnbpA-Fgγ construct. Right panel: schematic illustrating the molecular design of FnbpA-Fgγ construct ensuring the native pulling geometry from the C-terminus of the FnbpA and the N-terminus of Fgγ. (h) Representative bead height-time trace of FnbpA-Fgγ complex at a force around 4.0 ± 0.4 pN at 23 °C. (i) Representative bead height-time trace of FnbpA-Fgγ complex at a force around 20.0 ± 2.0 pN at 23 °C. Raw data and smoothed data using FFT with 10 points of window are indicated by gray and red, respectively. In this pulling geometry of the three homologue systems, the dissociation of the adhesion complex leads to the release of GS linker, while the N2, N3 domain are not under force. Hence, there was only one step corresponding to the dissociation of the complex.

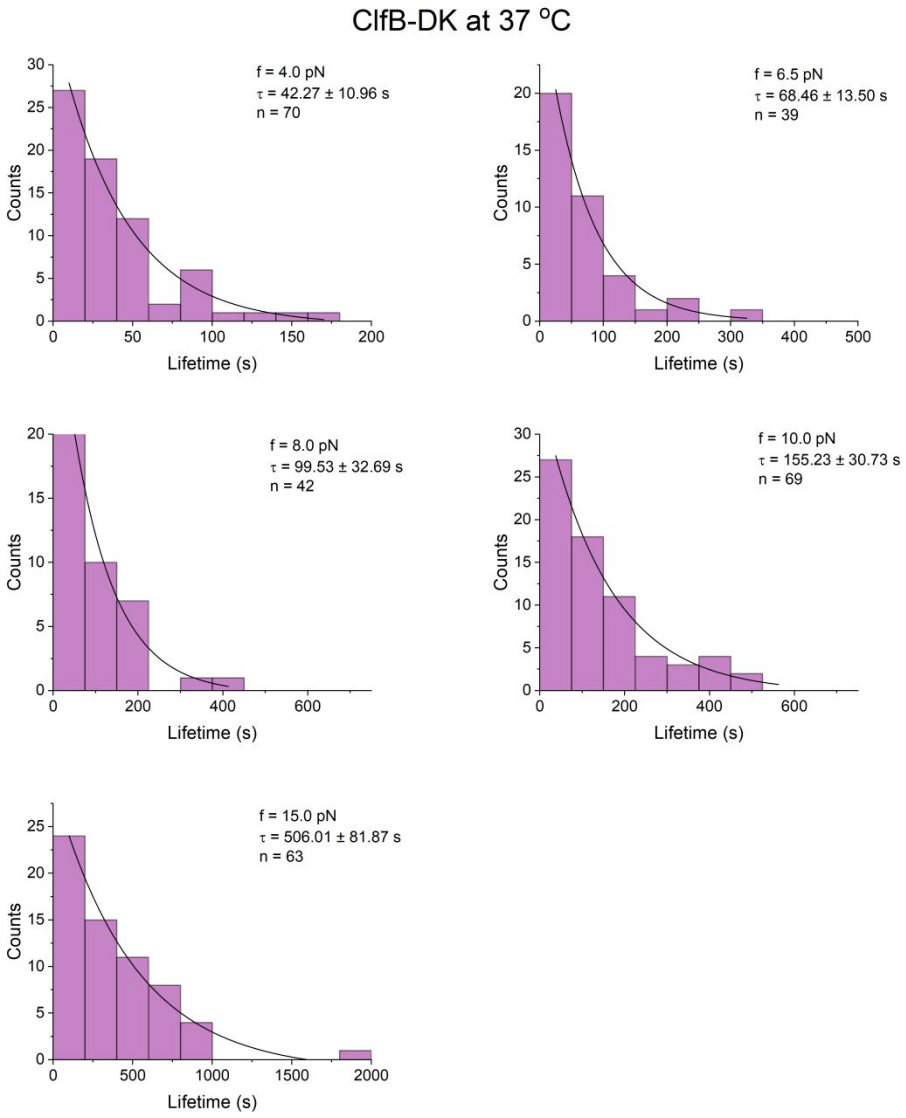

Figure S28. Lifetime histograms of ClfB-DK complex in the force range from 4.0 ± 0.4 pN to 15.0 ± 1.5 pN at 37 °C. The lifetimes at different forces are collected from 9 different tethers. Exponential decay function was used to fit each of the distribution (black curves) to obtain an average lifetime at each force. The applied average constant force (f), the average lifetime (τ), and number of the collected rupture events (n) at each force are shown in the figure.

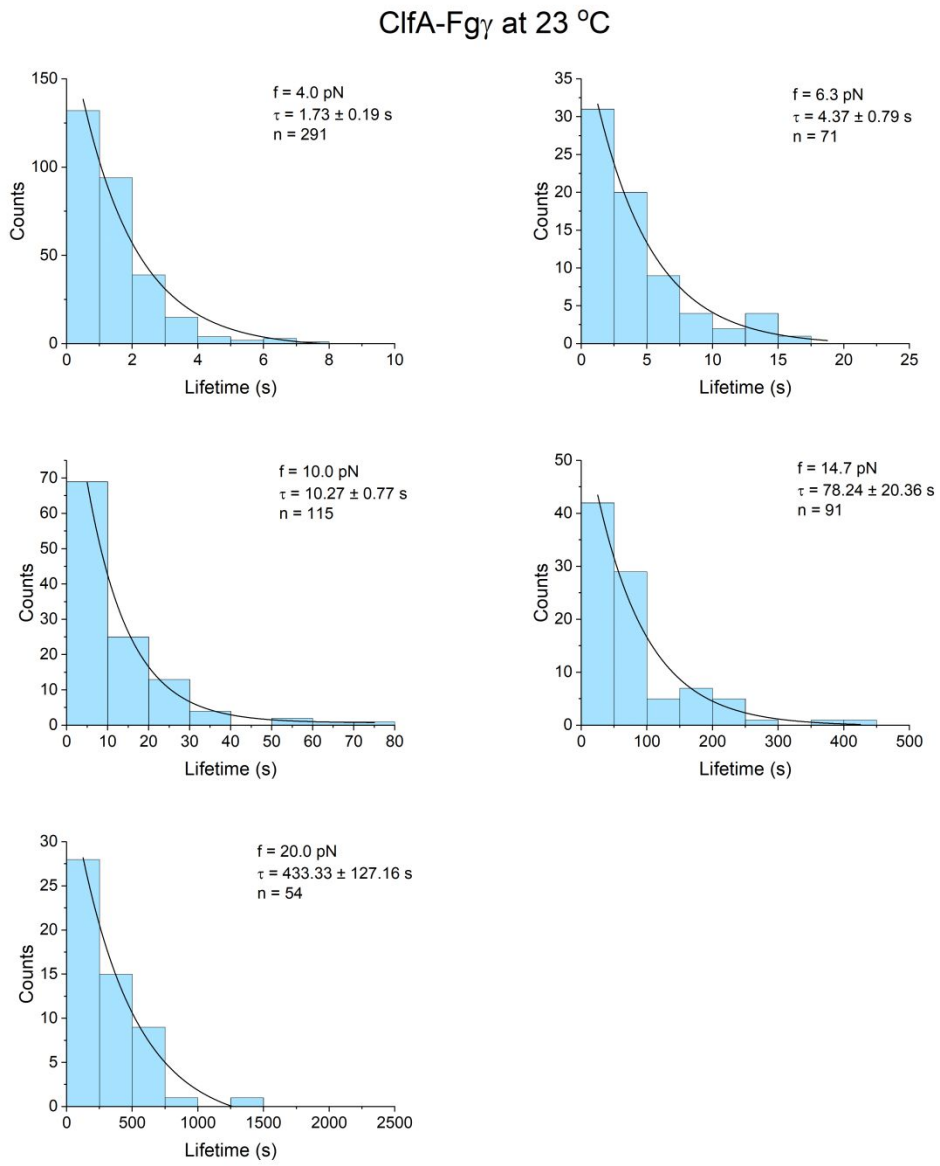

Figure S29. Lifetime histograms of ClfA-Fgγ complex in the force range from 4.0 ± 0.4 pN to 20.0 ± 2.0 pN at 23 °C. The lifetimes at different forces are collected from six different tethers. Exponential decay function was used to fit each of the distribution (black curves) to obtain an average lifetime τ at different forces. The applied average constant force (*f*), the average lifetime (τ), and number of the collected rupture events (*n*) at each force are shown in the figure.

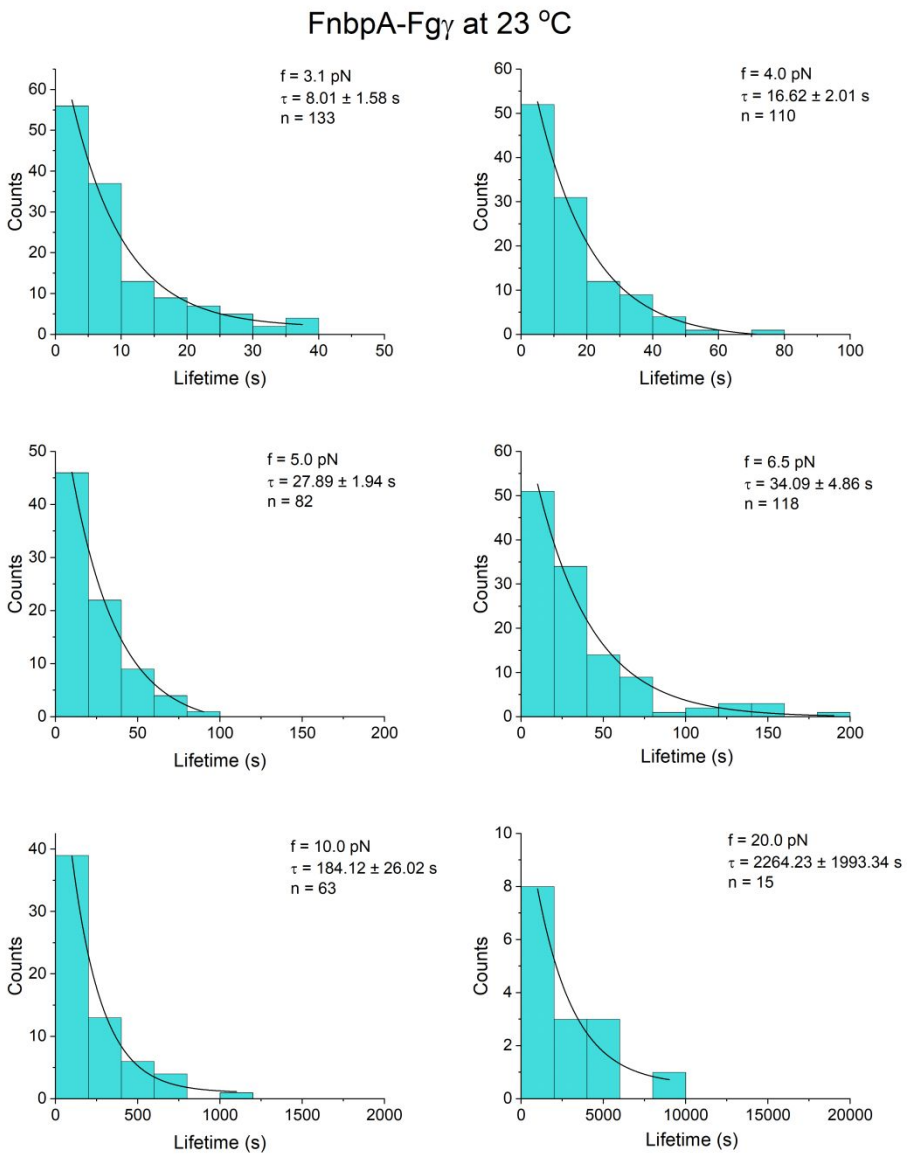

Figure S30. Lifetime histograms of FnbpA-Fgγ complex in the force range from 3.1 ± 0.4 pN to 20.0 ± 2.0 pN at 23 °C. The lifetimes at different forces are collected from three different tethers. Exponential decay function was used to fit each of the distribution (black curves) to obtain an average lifetime τ at different forces. The applied average constant force (*f*), the average lifetime (τ), and number of the collected rupture events (*n*) at each force are shown in the figure.

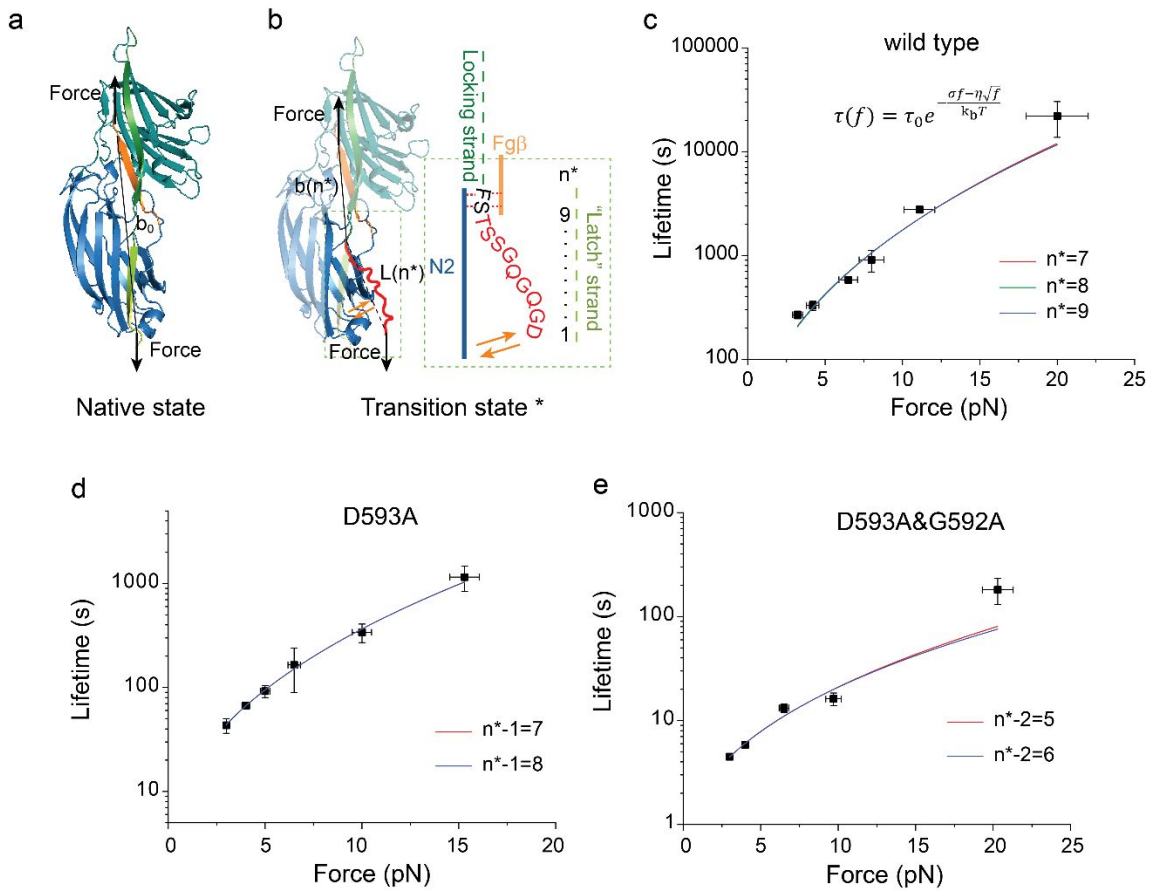

Figure S31. The structural-elastic determinant of the catch-bond kinetics. (a) The structure of the SdrG-Fgβ complex at native state, and (b) the proposed transition state, where the "latch" strand (residue 585-593, red) dissociate away from the N2 domain. b_0 and $b(n^*)$ indicate the linear distances between the two force attaching points on the rigid folded structural cores on the native and the transition states, respectively. $L(n^*)$ is the contour length of the "latch" peptide polymer unbinding from the N2 domain at the transition state. $b(n^*)$ and $L(n^*)$ are functions of the number of the released residues on the "latch" peptide at the transition state. (c) Force-dependent lifetimes of wild type SdrG-Fgβ complex at 23 °C fitted by the structural-elastic model suggest that n^* of 7-9 residues at the transition state (Table S2, Supporting Text 6). (d) Force-dependent lifetimes of D593A at 23 °C fitted by the structural-elastic model suggest that $n^* - 1$ of 7-8 residues at the transition state (Table S3, Supporting Text 6). (e) Force-dependent lifetimes of D593A&G592A at 23 °C fitted by the structural-elastic model suggest that $n^* - 2$ of 5-6 residues at the transition state (Table S4, Supporting Text 6).

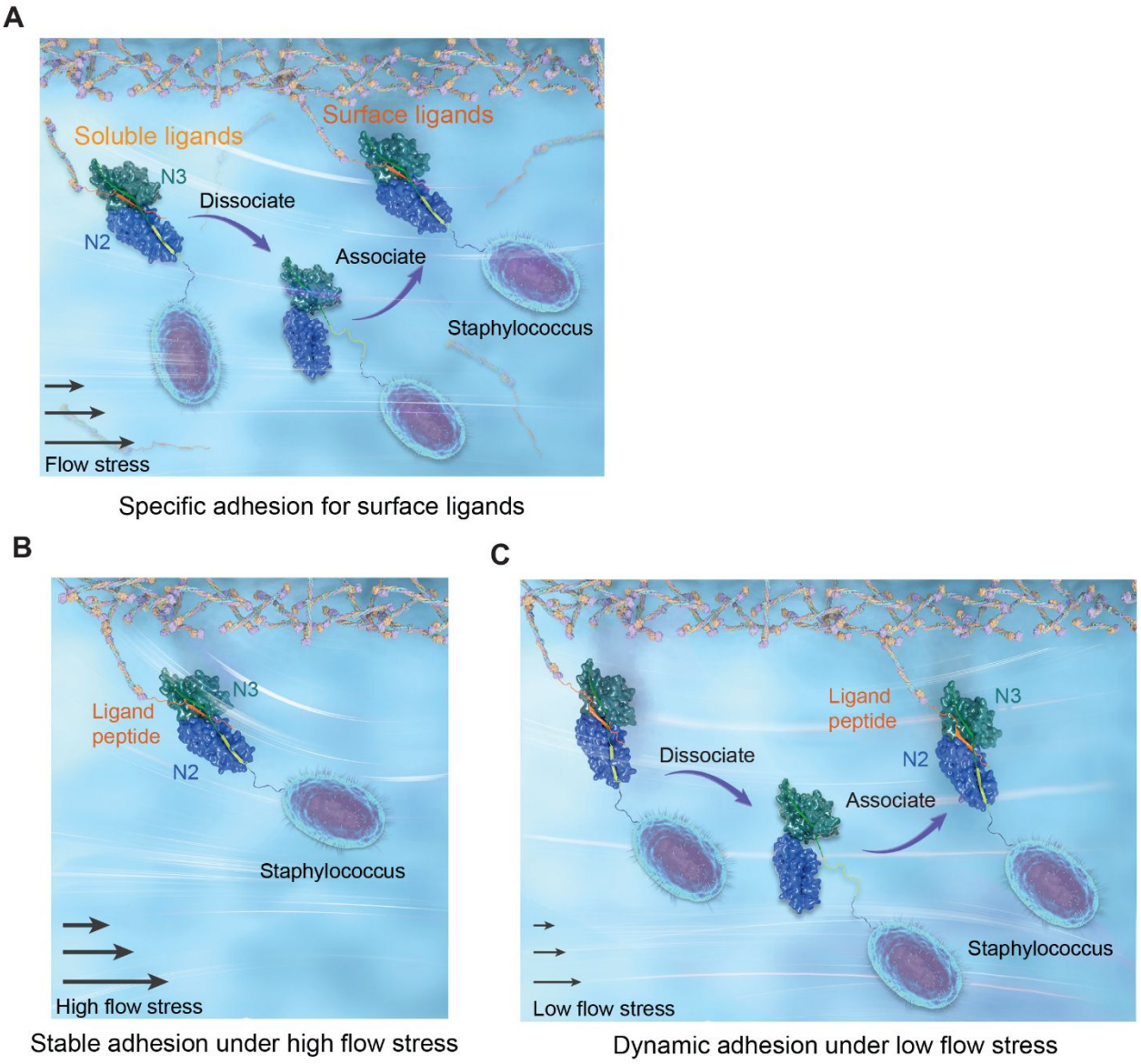

Figure S32. Proposed mechanisms of MSCRAMMs-mediated adhesion of the Staphylococcus pathogens. (A) An illustration of selective adhesion of Staphylococcus pathogens to surface immobilized ligands under flow stress conditions. Adhesions formed with soluble ligands quickly dissociate due to the lack of mechanical stabilization. **(B)-(C)**, The MSCRAMMs-mediated adhesion provides stable adhesion for the Staphylococcus pathogens to the surface under high flow stress condition, whereas it allows dynamic adhesion for the Staphylococcus pathogens to spread over the surface under low flow stress condition.

Table S1. Summary of the best-fitting parameters including dissociation lifetimes (τ_0) and transition distances ($\Delta x^{\ddagger}$) extrapolated from the force-dependent average lifetimes by the Bell's model. Means ± standard error.

Adhesion complex	Temperature (°C)	τ_0 (s)	$\Delta x^{\ddagger}$ (nm)	R-Square
SdrG-Fgβ wt	23 °C	97.24 ± 12.49	−1.20 ± 0.07	0.96257
SdrG-FFSARG	23 °C	54.44 ± 4.53	−1.37 ± 0.09	0.94977
SdrG-FgβdN4	23 °C	95.40 ± 4.27	−1.07 ± 0.03	0.99535
SdrG-FgβdC5	23 °C	96.15 ± 14.11	−1.29 ± 0.09	0.97394
SdrG-FgβF1	23 °C	18.01 ± 0.92	−1.16 ± 0.03	0.98758
SdrG-FgβF3	23 °C	211.16 ± 62.77	−1.29 ± 0.03	0.90419
SdrG_D593A-Fgβ	23 °C	23.07 ± 1.58	−1.08 ± 0.05	0.95494
SdrG_G592A+D593A-Fgβ	23 °C	2.47 ± 0.32	−0.87 ± 0.10	0.88447
SdrG_dC8-Fgβ	23 °C	9.77 ± 1.12	−0.68 ± 0.04	0.91797
SdrG-Fgβ wt	26.5 °C	22.00 ± 2.15	−1.12 ± 0.03	0.97971
	30 °C	12.30 ± 3.50	−1.04 ± 0.14	0.72739
	34 °C	5.09 ± 0.56	−0.98 ± 0.04	0.95101
	37 °C	1.97 ± 0.34	−0.89 ± 0.06	0.76415
SdrE-CFH	37 °C	3.29 ± 0.16	−1.75 ± 0.04	0.99422

Bbp-Fgα	37 °C	2.75 ± 0.35	−1.16 ± 0.07	0.91741
ClfB-DK	37 °C	16.04 ± 0.81	−0.99 ± 0.02	0.99713
ClfA-Fgγ	23 °C	0.46 ± 0.11	−1.30 ± 0.11	0.9562
FnbpA-Fgγ	23 °C	3.92 ± 0.95	−1.47 ± 0.16	0.85324

Table S2. Summary of the best-fitting parameters including the structural-elastic parameters (η) and extrapolated zero-force lifetime (τ_0) by fitting the force-dependent average lifetimes of wild-type SdrG-Fgβ with the structural-elastic model. $b^* - b_0$ is measured in the natively complex structure (PDB 1r17), L^*, and σ are calculated for a set of testing values of $n^* = 1 - 10$. Persistence length A is calculated at each testing n^*. Means ± standard error of the fitting.

n^*	$b^* - b_0$ (nm)	$L^* = 0.36 \times n^*$ (nm)	σ (nm)	η	A (nm)	τ_0 (s)	R-Square
1	−0.35	0.36	0.01	6.43 ± 0.74	~0.01	12.65 ± 5.93	0.89
2	−0.71	0.72	0.01	6.43 ± 0.74	~0.05	12.65 ± 5.93	0.89
3	−1.05	1.08	0.03	6.54 ± 0.74	~0.11	12.25 ± 5.80	0.89
4	−1.41	1.44	0.03	6.54 ± 0.74	~0.20	12.25 ± 5.80	0.89
5	−1.67	1.80	0.13	7.06 ± 0.78	~0.27	10.44 ± 5.20	0.88
6	−2.03	2.16	0.13	7.06 ± 0.78	~0.38	10.44 ± 5.20	0.88
7	−2.37	2.52	0.15	7.15 ± 0.79	~0.51	10.12 ± 5.10	0.88
8	−2.69	2.88	0.19	7.37 ± 0.81	~0.63	9.46 ± 4.86	0.88
9	−3.07	3.24	0.17	7.26 ± 0.80	~0.82	9.80 ± 4.99	0.88
10	−3.33	3.60	0.27	7.79 ± 0.84	~0.88	8.32 ± 4.44	0.87

Table S3. Summary of the best-fitting parameters including the structural-elastic parameters (η) and extrapolated zero-force lifetime (τ_0) by fitting the force-dependent average lifetimes of D593A with the structural-elastic model. $b^* - b_0$ is measured in the complex structure (PDB 1r17) by assuming the mutation totally disrupt the interaction between D593 to N2, L^*, and σ are calculated for a set of testing values (starts from G592) of $n^* = 1 - 9$. Persistence length A is calculated at each testing n^*. Means ± standard error of the fitting.

n^*	$b^* - b_0$ (nm)	$L^* = 0.36 \times n^*$ (nm)	σ (nm)	η	A (nm)	τ_0 (s)	R-Square
1	−0.36	0.36	0.0	5.98 ± 0.12	~0.02	3.59 ± 0.23	0.99
2	−0.7	0.72	0.02	6.09 ± 0.13	~0.06	3.47 ± 0.23	0.99
3	−1.06	1.08	0.02	6.09 ± 0.13	~0.13	3.47 ± 0.23	0.99
4	−1.32	1.44	0.12	6.63 ± 0.14	~0.19	2.95 ± 0.21	0.99
5	−1.68	1.80	0.12	6.63 ± 0.14	~0.30	2.95 ± 0.21	0.99
6	−2.02	2.16	0.14	6.73 ± 0.14	~0.42	2.85 ± 0.21	0.99
7	−2.34	2.52	0.18	6.95 ± 0.15	~0.54	2.67 ± 0.21	0.99
8	−2.72	2.88	0.16	6.84 ± 0.14	~0.73	2.76 ± 0.21	0.99
9	−2.98	3.24	0.26	7.38 ± 0.16	~0.79	2.34 ± 0.20	0.99

Table S4. Summary of the best-fitting parameters including the structural-elastic parameters (η) and extrapolated zero-force lifetime (τ_0) by fitting the force-dependent average lifetimes of D593A&G592A with the structural-elastic model. $b^* - b_0$ is measured in the complex structure (PDB 1r17) by assuming the mutation totally disrupt the interaction from D593 and G592 to N2, L^*, and σ are calculated for a set of testing values (starts from Q591) of $n^* = 1 - 8$. Persistence length A is calculated at each testing n^*. Means ± standard error of the fitting.

n^*	$b^* - b_0$ (nm)	$L^* = 0.36 \times n^*$ (nm)	σ (nm)	η	A (nm)	τ_0 (s)	R-Square
1	−0.34	0.36	0.02	4.55 ± 0.58	~0.03	0.67 ± 0.20	0.89
2	−0.7	0.72	0.02	4.55 ± 0.58	~0.10	0.67 ± 0.20	0.89
3	−0.96	1.08	0.12	5.02 ± 0.60	~0.19	0.58 ± 0.18	0.89
4	−1.32	1.44	0.12	5.02 ± 0.60	~0.34	0.58 ± 0.18	0.89
5	−1.66	1.80	0.12	5.02 ± 0.60	~0.53	0.58 ± 0.18	0.89
6	−1.98	2.16	0.18	5.31 ± 0.61	~0.68	0.54 ± 0.17	0.88
7	−2.36	2.52	0.16	5.21 ± 0.60	~0.96	0.55 ± 0.17	0.88
8	−2.62	2.88	0.26	5.69 ± 0.62	~1.05	0.49 ± 0.16	0.88

Table S5. Comparison of the catch-bond kinetics based on the catch-to-slip switch force (f_s), the largest lifetime at the switch force ($\tau(f_s)$), and the ranges of lifetime changed by force.

Biomolecular system	f_s (pN)	$\tau(f_s)$ (s)	Tested force ranges (pN)	Lifetime increase ranges (s)
SdrG-Fgβ	>> 50*	> 10^6*	3−30	10^2−10^5
PSGL-1/P-selectin[17]	~ 25	~ 1.2	10−25	0.2−1.2
FimH/mannose-BSA[18]	30−70	< 5		
E-cadherin dimer[16]	~ 30	~ 0.1	10−30	0.02−0.1
cadherin-catenin complex/F-actin[19]	~ 8	~ 1.3	4−8	0.4−1.2
Integrin $\alpha_v\beta_1$/FNIII7-10[20]	~ 30	~ 5	4−30	~0.1−5
T12 vinculin/F-actin[21]	~ 8	~ 12	1−8	~ 0.1−12
TCR/pMHC (by BFP)[22]	~10	~0.8	0−10	0.2−0.8
TCR/pMHC (by Optical Tweezer)[23]	~15	~3.5	5−15	~0.5−3.5
Titin Ig27[15]	~20	~10^4	~4-20	~10^3−10^4

* the catch-to-slip switch of SdrG-Fgβ complex was not directly observed in our experiment due to the drastically increased lifetime.

References

1 Chen, H. *et al.* Improved high-force magnetic tweezers for stretching and refolding of proteins and short DNA. *Biophys. J.* **100**, 517-523 (2011).

2 Zhao, X., Zeng, X., Lu, C. & Yan, J. Studying the mechanical responses of proteins using magnetic tweezers. *Nanotechnology* **28**, 414002 (2017).

3 Bustamante, C., Marko, J. F., Siggia, E. D. & Smith, S. Entropic elasticity of lambda-phage DNA. *Science* **265**, 1599-1600 (1994).

4 Dietz, H. & Rief, M. Protein structure by mechanical triangulation. *Proc. Natl. Acad. Sci. U.S.A.* **103**, 1244-1247 (2006).

5 Yu, M. *et al.* Effects of Mechanical Stimuli on Profilin- and Formin-Mediated Actin Polymerization. *Nano Lett.* **18**, 5239-5247 (2018).

6 Chen, H. *et al.* Dynamics of Equilibrium Folding and Unfolding Transitions of Titin Immunoglobulin Domain under Constant Forces. *J. Am. Chem. Soc.* **137**, 3540-3546 (2015).

7 Schönfelder, J., Perez-Jimenez, R. & Muñoz, V. A simple two-state protein unfolds mechanically via multiple heterogeneous pathways at single-molecule resolution. *Nat. Commun.* **7**, 11777 (2016).

8 Williams, P. M. *et al.* Hidden complexity in the mechanical properties of titin. *Nature* **422**, 446-449 (2003).

9 Williams, M. C., Rouzina, I. & McCauley, M. J. Peeling back the mystery of DNA overstretching. *Proc. Natl. Acad. Sci. USA* **106**, 18047-18048 (2009).

10 Zhang, X. *et al.* Revealing the competition between peeled ssDNA, melting bubbles, and S-DNA during DNA overstretching by single-molecule calorimetry. *Proc. Natl. Acad. Sci. USA* **110**, 3865-3870 (2013).

11 Yu, M., Lu, J.-H., Le, S. & Yan, J. Unexpected Low Mechanical Stability of Titin I27 Domain at Physiologically Relevant Temperature. *J. Phys. Chem. Lett.* **12**, 7914-7920 (2021).

12 Le, S., Yu, M. & Yan, J. Mechanical regulation of tension-transmission supramolecular linkages. *Curr. Opin. Solid State Mater. Sci.* **25**, 100895 (2021).

13 Yuan, G. *et al.* Elasticity of the Transition State Leading to an Unexpected Mechanical Stabilization of Titin Immunoglobulin Domains. *Angew. Chem. Int. Ed.* **56**, 5490-5493 (2017).

14 Guo, S. *et al.* Structural–elastic determination of the force-dependent transition rate of biomolecules. *Chem. Sci.* **9**, 5871-5882 (2018).

15 Guo, S., Efremov, A. K. & Yan, J. Understanding the catch-bond kinetics of biomolecules on a one-dimensional energy landscape. *Commun. Chem.* **2**, 1-9 (2019).

16 Rakshit, S. *et al.* Ideal, catch, and slip bonds in cadherin adhesion. *Proc. Natl. Acad. Sci. USA* **109**, 18815-18820 (2012).

17 Marshall, B. T. *et al.* Direct observation of catch bonds involving cell-adhesion molecules. *Nature* **423**, 190-193 (2003).

18 Le Trong, I. *et al.* Structural Basis for Mechanical Force Regulation of the Adhesin FimH via Finger Trap-like β Sheet Twisting. *Cell* **141**, 645-655 (2010).

19 Buckley, C. D. *et al.* The minimal cadherin-catenin complex binds to actin filaments under force. *Science* **346** (2014).

20 Kong, F. *et al.* Demonstration of catch bonds between an integrin and its ligand. *J. Cell Biol.* **185**, 1275-1284 (2009).

21 Huang, D. L. *et al.* Vinculin forms a directionally asymmetric catch bond with F-actin. *Science* **357**, 703-706 (2017).
22 Liu, B., Chen, W., Evavold, Brian D. & Zhu, C. Accumulation of Dynamic Catch Bonds between TCR and Agonist Peptide-MHC Triggers T Cell Signaling. *Cell* **157**, 357-368 (2014).
23 Das, D. K. *et al.* Force-dependent transition in the T-cell receptor β-subunit allosterically regulates peptide discrimination and pMHC bond lifetime. *Proc. Natl. Acad. Sci. USA* **112**, 1517-1522 (2015).